

Understanding Multicomponent classification behavior in a Hydrocyclone

Mandakini Padhi

**A Dissertation Submitted to
Indian Institute of Technology Hyderabad
In Partial Fulfillment of the Requirements for
The Degree of Master of Technology**



भारतीय प्रौद्योगिकी संस्थान हैदराबाद
Indian Institute of Technology Hyderabad

**Department of Chemical Engineering
Indian Institute of Technology, Hyderabad**

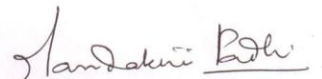
June, 2015

Declaration

I declare that:

- The work contained in this report is original and has been done by me under the guidance of my supervisor.
- The work has not submitted to any other Institute for any Degree or Diploma.
- I have followed the guidelines provided by the Institute in preparing the report.
- I have conformed to the norms and guidelines given in the Ethical code of conduct of the Institute.
- Whenever I have used any data, theoretical analysis, figures, tables and texts from other sources, I have given due credit to them by citing them in the report and giving their details in the references.

30 June, 2015


Mandakini Padhi
Ch13m1008

Approval Sheet

This thesis entitled “*Understanding multicomponent classification behavior in a Hydrocyclone*” by Mandakini Padhi is approved for the degree of Master of Technology from IIT Hyderabad.



Dr. Sunil Kumar Maity
Examiner



Shri K. Anand Rao
BARC-AMD, Hyderabad
External Examiner



Dr. Narasimha Mangadoddy
Adviser



Dr. Raja Banerjee
Chairman

Acknowledgements

“It is the supreme art of the teacher to awaken joy in creative expression and knowledge” -Albert Einstein

I take this opportunity to express my profound gratitude and deep regards to my guide Dr. M Narasimha, Asst. Professor, Department of Chemical Engineering, IIT Hyderabad for his exemplary guidance, monitoring and tireless pursuit for academic excellence throughout my M. Tech course. The blessing, help and guidance given by him time to time shall carry me a long way in the journey of life on which I am about to embark. He has been a constant source of courage and support throughout my M. Tech course.

I express my heartfelt respect and sincere gratitude to NMDC – R&D Hyderabad and BARC- AMD Hyderabad for providing me with the resources and guidance which helped me in completing the project. The wonderful research facilities along with a friendly work culture constantly motivated me to carry out my research work in a decent pace.

I am privileged to express my deep sense of gratitude and heartfelt thanks to Mr. VTSR Kumar Reddy, PhD scholar, IIT Hyderabad for his valuable guidance, vehement personal interest and stepping forward to be lend me hand for all new fields I entered to explore. I am equally indebted to Department of Chemical Engineering, IIT Hyderabad, for providing every support required during my research activities.

On the personal front, I'm grateful to my Parents, Mr. Umakant Padhi and Mrs. Ashalata Padhi for their blessings, love, sacrifice and constant support without which, I would not have been where I am today. No words are sufficient to acknowledge the love, care and support that I have always received from my brother, Krushna Chandra Padhi; sister, Madhuri Padhi and friend Shashwat Bhowmic. Their constant prayers, words of encouragement and the strong bond of trust have helped me achieve my aims in life. Without them I would not have existed. I am forever indebted to them.

Mandakini Padhi

Dedicated to..

My family.

Abstract

In most mineral comminution circuit, the feed to the hydrocyclone classifier is composed of a mixture of particles having varying degrees of liberation and sizes. The different liberation degree for the minerals leads to multi density particles that are significantly differ in hydrocyclone during the classification. Hydrocyclone classifier performance calculation till now is based on single average mineral density component behavior, contradicting to the actual situation of naturally occurring ores. Therefore, present work is aimed to study the separation by size wise component classification curves of hydrocyclone operation including the study of varying density components. This involves on varying set of parameters i.e. spigot, pressure, cone angle and feed solid content. The initial studies is done with bicomponent mixture of pure magnetite and silica with 5 proportions 1:9, 2:8, 1:1, 8:2, 9:1 (silica: magnetite) conducted in 2 inch hydrocyclone. Further, this also includes the 3 inch hydrocyclone classification multicomponent studies, using naturally occurring iron ore slimes which have iron, alumina and silica as 3 compositions. The component analysis of iron ore has been done by combination of volumetric analysis, X-ray fluorescence (XRF), Inductively Coupled Plasma Mass Spectrometry (ICP-OES) and gravimetric method for ensuring the size-wise distribution of the Fe_2O_3 , Al_2O_3 and Si_2O in respective streams after separation. A set of optimized hydrocyclone operation is identified for the iron ore slimes beneficiation suitable for pellet grade product.

Followed by experiments, a number of CFD simulations on hydrocyclone treating bi-component feed mixture were conducted. The turbulence model is solved using the RSM and LES for 2inch and 3inch hydrocyclone. The multiphase modeling is done using the VOF (volume of fluid) and ASM (Mixture Model). The simulation contains 10 phases at an instant i.e. water, air, 4 phases of magnetite and silica each of different sizes and volume fraction. The mixture of magnetite and silica i.e. 1:9, 2:8, 1:1 is considered for the understanding of interaction between components and sizes in complex flow system at optimized hydrocyclone conditions. The CFD model is able to predict the salient features of the cyclone flow fields in great detail, thus providing a better understanding of the solid recovery(R_s) to the underflow, where we have high R_s for the heavier

particle i.e. magnetite and vice-versa. The cut-size (d_{50}) is observed as lower for the heavier particle compared to the lighter particles and the mixtures.

Validation of the previously developed multi-component classification mathematical model by Narasimha et al., 2014 is made against the newly supplemented data on bi and multi-component hydrocyclone performance. Predictions of the component reduced cut size and solid recovery for bi-component system are seem to reasonably close to experimental data.

Nomenclature

C_D :	Drag coefficient
v_r, u_r :	Radial velocities
v_θ :	Angular velocity
ρ_f :	Fluid Density
ρ_s :	Particle Density
Ac:	Cross-sectional Area
S:	Volumetric flow split
Du:	Underflow Diameter
Do:	Overflow Diameter
Dc:	Cylindrical Diameter
Lc:	Length of cylindrical portion
H:	Slurry feed head,
H:	Vortex finder to spigot distance,
φ :	Volume fraction of solids in feed,
a, b, c, d, f, g	Empirical constants.
d_{50} :	Cut size
Q :	Flow rate of slurry.
C_v :	Volumetric fraction of solid in feed slurry(%)
K_{dl} :	Constant depends on feed
P :	Pressure.
K_w :	Constant depends on feed property
V_h and V_t :	Hindered and tangential velocity,
i :	Cone angle
μ_m / μ_w :	Viscosity of mixture / water
f_v :	Solid fraction of slurry
Re:	Reynold's No
x_i :	Distance in i-direction
μ :	Molecular viscosity
S_{ij} :	Strain rate tensor

u_i :	Velocity components in i-direction, instantaneous velocity
u_i' :	Fluctuation velocity
U_i :	Mean velocity
$D_{L,ij}$:	Molecular viscous diffusion term
P_{ij} :	Stress production term
F_{ij} :	Rotation production
$C1, C2$:	Constants
k :	Turbulent kinetic energy,
ε :	Turbulent dissipation rate
μ_t :	Turbulent viscosity coefficient
\dot{m}_{qp} :	Mass transfer from phase q to phase p
\dot{m}_{pq} :	Mass transfer from p to q phase
u_{km} :	Drift velocity of the phase k
u_{kc} :	Slip velocity of the dispersed phase k
τ_{ij} :	Turbulent stresses in the tensor
WR – CC :	without rod and cone changed(10^0)
WR –	without Rod and old cone (12^0)
R –	With Rod and old cone (12^0)

Table of contents

Declaration	
Approval sheet	
Acknowledgement	
Abstract	
Nomenclature	
List of figures	
List of Table	
Introduction	1
1.1 <i>Background</i>	1
1.1.1 Hydrocyclone and its operation.....	1
1.2 <i>Hydrocyclone performance and Multicomponent behavior</i>	2
1.3 <i>Importance of work</i>	3
1.3.1 Industrial Application	3
1.3.2 Bi-component and Multicomponent Behavior.....	4
1.4 <i>Scope of Work</i>	5
Literature Review	6
2.1 <i>Hydrocyclone Mathematical Models</i>	6
2.1.1 Model Limitations	9
2.2 <i>Multicomponent separation concepts and Models:</i>	10
2.3 <i>Iron ore beneficiation</i>	12
2.4 <i>CFD modeling for the hydrocyclones</i>	13
2.4.1 Turbulence	13
2.4.2 Multiphase model	14
Methodology	18
3.1 <i>Bi-component Experiment Methodology:</i>	18
3.2 <i>Iron Ore Slime Experiment Methodology:</i>	20
3.2.1 Hydrocyclone Test Rig for Iron ore experiment.....	21
3.2.2 Hydrocyclone Experiments	22
3.2.3 Size wise Characterization Approach	23
3.3 <i>CFD Methodology</i>	25
3.3.1 Cyclone geometry and grid generation.....	25

3.3.2 Boundary condition :	26
3.3.3 CFD Modeling.....	26
4.1 <i>Bi component (silica and magnetite) hydrocyclone experiments</i>	32
4.1.1 <i>Experiments with feed slurry:</i>	32
4.2 <i>Iron ore slime Hydrocyclone experiments and Analysis</i>	45
4.2.1 Silica Slurry experiments: Design selection	45
4.2.2 Water split	47
4.2.3 Solids recovery (Rs):	48
4.2.4 Performance behavior of components:	48
4.2.5 Effect of Various designs (Du and cone angle Vs D_{50}):	51
CFD Simulation – Results and Discussions	52
5.1 <i>Two phase flow field:</i>	52
5.2 <i>Three inch Hydrocyclone simulations</i>	57
Multicomponent Classification Model testing	65
6.1 <i>Cut size model:</i>	65
6.2 <i>Sharpness of separation:</i>	65
6.3 <i>Solid Recovery model:</i>	66
Conclusion and Future work	68
7.1 <i>Conclusion</i>	68
7.1.1 Bi component studies:.....	68
7.1.2 Iron Ore Slime Studies:	68
7.1.3 CFD Simulations:	69
7.1.4 Multicomponent Model Validation:.....	69
7.2 <i>Future work</i>	69

List of Figures

Figure 1.1: Schematic of Hydrocyclone.....	2
Figure 1.2: Ball Mill - Hydrocyclone Circuit Figure 1.0.3: Hydrocyclone Ball Mill Circuit.....	4
Figure 2.1: Dimensional details of hydrocyclone	7
Figure 2.2: Comparison of predicted tangential velocities with experimental results for the 75mm hydrocyclone at 60mm from the roof of the cyclone wall (Narasimha 2006)	144
Figure 3.1: Design of experiment for 2 inch hydrocyclone - Bicomponent studies	19
Figure 3.2: Alumina and silica distributions	20
Figure 3.3: 1. Average analysis (-34) and 2. Spot analysis(+54) - SEM.....	21
Figure 3.4: Schematic Diagram : Experimental set up of Hydrocyclone.....	222
Figure 3.5: 3inch Hydrocyclone Mesh	266
Figure 3.6: 2 inch Hydrocyclone Mesh.....	26
Figure 3.7: Mean and fluctuating velocity	28
Figure 4.1: Flow rate Vs Pressure variation (2 inch -8VF).....	32
Figure 4.2: Flow rate Vs pressure variation (2 inch-11 VF).....	33
Figure 4.3: Actual efficiency curve - comparison of two experiments.....	37
Figure 4.4: Actual efficiency curve - Comparison of two experiments.....	37
Figure 4.5 : d_{50} (At 10%) Vs Proportions.....	38
Figure 4.6: d_{50} (At 5%) Vs Proportions.. ..	38
Figure 4.7: d_{50} Vs Spigots diameter (1:9) 5 % solids.....	39
Figure 4.8 : d_{50} Vs Spigots diameter (1:1) 5% solids.....	40
Figure 4.9 : d_{50} Vs Spigots diameter (9:1) 5% solids.....	40
Figure 4.10: Force ratio (Do/Du) effect on d_{50} (10% solids).....	41
Figure 4.11: R_s Vs Component Composition.....	42
Figure 4.12 : R_f Vs Different Component compositions at 5% solids.....	43
Figure 4.13: Actual efficiency curve: 10% solid, 1:1 (Mag:Silica).....	43
Figure 4.14: Actual Efficiency curve : 5% solid 1:1 (mag:Silica).....	44
Figure 4.15: Silica slurry partition curve with different hydrocyclone designs.....	46
Figure 4.16: Water Split Vs DOEs.....	47
Figure 4.17: Solid Recovery Vs different Designs.....	48
Figure 4.18: Tega hydrocyclone (spigot 17.5 / cone 12 ⁰) - E_a	49
Figure 4.19: Tega hydrocyclone(spigot: 17.5/ cone: 10 ⁰)- E_a	50

Figure 4.20: Tega hydrocyclone (spigot :25 / cone : 12 ⁰)- Ea.....	50
Figure 4.21: Du and cone angle Vs D50.....	51
Figure 5.1: Tangential velocities by different meshes at 470 mm from top of the cyclone using RSM and VOF model in 3 inch.....	53
Figure 5.2: Axial velocities by different meshes at 470 mm from top of the cyclone using RSM and VOF model in 3 inch.....	54
Figure 5.3: Air –core formation in 3inch and 2 inch Hydrocyclone.....	55
Figure 5.4: Turbulence Intensity in 3inch and 2 inch Hydrocyclone.....	55
Figure 5.5: Comparison of experimental and CFD plots flow rate Vs Pressure in 2 inch hydrocyclone (6.4 mm Du).....	56
Figure 5.6: Comparison of experimental and CFD plots Water split Vs Pressure in 2 inch hydrocyclone (6.4 mm Du).....	56
Figure 5.7: water split comparison at different pressures in 3inch hydrocyclone (only water Experiment).....	57
Figure 5.8 : Comparison of 2inch and 3 inch hydrocyclone Aircore - water interface.....	57
Figure 5.9: Volume fraction contours of silica(left) and magnetite (right) at (a) 2.75 micron, (b) 11 micron, (c) 22 micron and (d) 52.32 micron (From a mixture of 1:1- silica and magnetite)..	58
Figure 5.10: LZVV of various proportions of magnetite.....	59
Figure 5.11: Tangential velocity at different proportion at 600 mm from top of hydrocyclone(near spigot).....	60
Figure 5.12:Tangential velocity at different proportion at 300 mm from top of hydrocyclone (near the cylindrical and conical junction).....	60
Figure 5.13: Contours for comparison of 52.32 micron size silica in underflow area (a) silica from 1:1 mixture and (b) Pure silica.....	61
Figure 5.14: Comparison of magnetite and silica distribution at vortex finder area (a), (b) in 50% and (c) pure silica (d) pure magnetite.....	62
Figure 5.15: Mean position of volume spread (a) silica and (b) magnetite in 1:1 proportion....	62
Figure 5.16 :mean position of volume spread (a)silica and (b)magnetite in 8:2 proportion.....	63
Figure 5.17: Mean position of volume fraction spread (a) pure silica and (b) pure magnetite....	64
Figure 6.1:d ₅₀ for the model fitting.....	66
Figure 6.2: Solid recovery for 5% and 10 % experiments.....	67
Figure 6.3: Sharpness of separation of silica comparisons with (Weller et al., 1988) and (Narasimha et al., 2014).....	67

List of Tables

Table 2-1: Summary of CFD modeling in hydrocyclone.....	16
Table 3-1: Design of Experiment for 2inch Hydrocyclone.....	18
Table 3-2: Iron ore slime compositions.....	20
Table 3-3: Design of experiments - 4 inch hydrocyclone.....	222
Table 3-4: 3 inch and 2 inch Cyclone dimensions	25
Table 4-1: Summary of Experiments and Results - 2Inch hydrocyclone	34
Table 4-2: Design of experiments (Iron ore Slime)	45
Table 4-3 : Solid % for 3inch Hydrocyclone (Iron ore slimes)	46
Table 4-4: Performance parameters analyzed from Iron ore Slimes experiment.....	49
Table 5.1: List of cases for feed input attempted for CFD simulation in 3 inch Hydrocyclone.....	52

Chapter 1

Introduction

1.1 Background

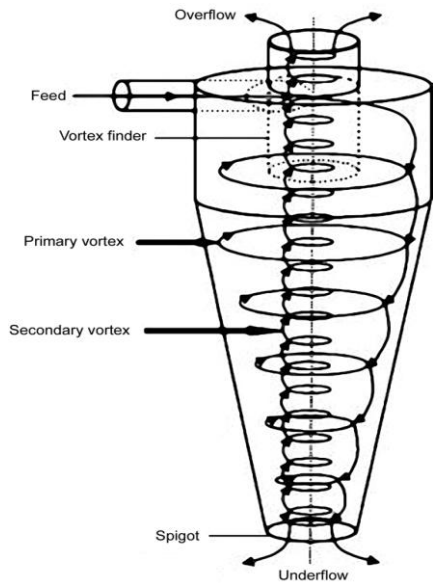
1.1.1 Hydrocyclone and its operation

A hydrocyclone is a static device that applies centrifugal force to a liquid mixture to promote the separation of heavy and light components. Because of its static operation, and high energy efficiency, it is vastly used in many industries like Mineral, chemical, pharmaceutical etc for classification purpose. Hydrocyclone are widely used in grinding circuits due to their high capacity and relatively high efficiency. This classifies very wide size range separation, typically from 5- 500 microns.

The hydrocyclone is a closed vessel designed to convert incoming liquid velocity into vortex motion. The feed enters tangentially into the cylindrical section of the hydrocyclone,

Figure 1.1, and follows a circulating path with a net inward flow of fluid from the outside to the vortex finder on the axis. The centrifugal field generated by the high circulating velocities creates an air core on the axis that usually extends on the spigot opening at the bottom of the conical section from the vortex finder at the top. In order to the air core to be form the centrifugal force field must be several times larger than the gravitational one and the pressure in the central axis must be lower than the atmospheric condition.

Particles that experience this centrifugal field will tend to move outwards relative to the carrier fluid because of their relatively greater density. The larger, heavier particles will migrate rapidly to the walls of the cylindrical section and will then be forced to move downward to the conical wall. Small particles will, on the other hand, be dragged inward by the fluid as it moves towards the vortex finder. The solid separation occurs in the passage of the suspension along the barrel of the hydrocyclone, to form thickened slurry at the outer wall, which than leaves the hydrocyclone as a continuous stream from its discharge-nozzle at the bottom.



The velocity of flow in the hydrocyclone can be resolved into three components namely tangential, axial and radial. Basically the hydrocyclone is subjected to two opposing forces – an outward centrifugal force and an inwardly acting drag force. The centrifugal force developed accelerates the settling rate of the particles and there by separating particles according to size and specific gravity.

Figure 1.1: Schematic of Hydrocyclone

Due to drag force the slower moving particle moves upward in the overflow along with water phase. There is a locus of zero vertical velocity (LZVV) inside the hydrocyclone I a similar shape of cone. Particle attains an equilibrium a position outside the LZVV, with higher tangential velocities goes to the underflow as heavy material and the inside particles go to the overflow. The particles on the LZVV are acted by equal forces of centrifugal and drag and have equal chances of reporting to the underflow and overflow and termed as the cut size (d_{50}), having equal probability to report in underflow and overflow.

1.2 Hydrocyclone performance and Multicomponent behavior

The performance of the hydrocyclone is shown by efficiency curve, which represents the weight fraction or percentage of each particle size in feed that reports to the underflow. Performance by means of cut-size (d_{50}), in ideal classification all the particles with size higher than the cut-size report to the underflow and those below escape through the overflow. But this is just hypothetical case. Always there is chance of misplacement of particle. This can be represented through sharpness of separation or imperfection.

Water split ratio is one more factor is of great importance. One can observe entrainment effect, which results in entrainment of fine material by liquid in underflow. This efficiency function can be considered to be the result of two parts. One is classification function which can be considered as the result of classifying action of hydrocyclone.

While the second is result of water split. The second function does not involve classification activity of hydrocyclone. Because of this it appears a changed hydrocyclone performance. So there is a need to correct this, which can be achieved by the use corrected efficiency curve as the indicator of performance of the hydrocyclone. This corrected efficiency curve is a smooth curve, which is “S” shaped which starts at zero at fine end and increases to 100% at coarse end. There are many cases when efficiency curve fails to show the ideal behavior. Multi component feed having different densities may be one of those kinds of situations, which is the key motivation for this work. With a heterogeneous feed containing the particles varying in density, individual feed component follow standard efficiency curve. But the combined curve deviates from standard “S” shape. If fraction of high density particles is known for each fraction, then using weighted averages it is possible to calculate the overall efficiency for each size fraction. The overall efficiency curve is dominated by high density component at lower sizes and by lighter component at high sizes with inflection.

1.3 Importance of work

1.3.1 Industrial Application

Mineral processing mainly consists of beneficiation of the raw ore into highly concentrated minerals ores to reduce the cost of the transportation and the further processing hence getting high efficiency. The two main processes that take place in the industries are extraction and separation of the minerals from the gauge. Hydrocyclone acts as key component in separation process. Usually it is put in the closed circuit with the ball milling to separate and liberate out the desired grounded materials from the mill outlet and recycle the ungrounded back to circuit. The Figure 1.2 shows the closed comminution circuit schematic, where hydrocyclone used as classifying equipment. In this the complex behavior of the hydrocyclone leads to some interesting behavior.

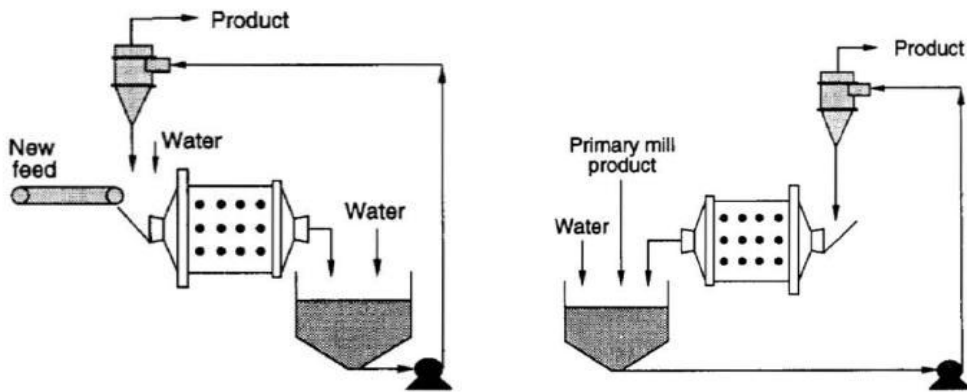


Figure 1.2: Ball Mill - Hydrocyclone Circuit **Figure 1.3: Hydrocyclone Ball Mill Circuit**

It has been observed that few of the fine material and high density material reports to the underflow, which is undesirable and increases the energy consumption of the milling process by increasing the load. It is due to the interference of the multicomponent present in the feed where because of wide range of density difference the misplacement of finer and heavier particle is found.

1.3.2 Bi-component and Multicomponent Behavior

The naturally occurring ore includes two and more components in it. During the milling and separation process these material interferes with each other due to different size and density at the same time. Hence it is very important to study the effects including the complex flow pattern in the hydrocyclone. Various studies with a limited data have shown the effects of the single average density effect of the component. Their work showed how the different density components are affecting the performance of hydrocyclone. Due to density difference between chromite particles and silicate particles, coarse silicate reports to the overflow and fine chromite reports to underflow. This causes high recirculation load of fine dense materials. (Kawatra, 2006), also tried to address these problems with study on inflections in hydrocyclone efficiency curves. Experimental evidences of influence of multicomponent particles on hydrocyclone efficiency curve have motivated the researchers to conceptualize the modeling of hydrocyclone performance based on multicomponent behavior. (Narasimha et al., 2012), attempted to develop single component model with average density. This model included additional term, a density function, which was flexible enough to extend that to

multicomponent classification model. (Narasimha et al, 2014), recently proposed a model including the effect to individual particle density and its effect on the mixture flow in classification phenomenon.

1.4 Scope of Work

The current study is aimed to understand the phenomenon of multicomponent classification in a hydrocyclone and the influence of different cyclone design and operating conditions on it. Understanding the component interaction is the key step in going for the model development. The CFD simulation is also aimed to understand the parametric studies and to define the interaction parameter of multicomponent in hydrocyclone. Using the generated bi-component experimental data, this work aims to validate the previously developed multicomponent classification model.

Chapter 2

Literature Review

2.1 Hydrocyclone Mathematical Models

Hydrocyclone have tangential input and it carries centrifugal force by producing a swirling motion at the same time drag force in counter to that, which can be shown as, (Eqn 2.1):

$$0.5C_D(v_r - u_r)2\rho_f A_c = \frac{v_\theta}{r} v_p(\rho_s - \rho_f) \quad (2.1)$$

$$\text{Drag force} = \text{Centrifugal force}$$

Where, C_D represents drag coefficient, v_r , u_r as radial velocities, v_θ , angular velocity

ρ_f : Fluid Density, ρ_s : Particle Density and A_c : Cross-sectional Area

The lighter particle goes to overflow by escaping the drag force equilibrium and the heavier to the underflow by the effect of centrifugal force in major and also gravitational force.

The hydrocyclone efficiency is measures by various parameters like cut-size d_{50} , sharpness of separation α , solid recovery to underflow R_s , water split R_f etc, as mentioned in chapter 1. The particle distribution inside hydrocyclone defines d_{50} , depending on which the particle can be tracked in overflow or underflow based on size. Particle having higher diameter than d_{50} reports to underflow and vice-versa.

No one set of assumptions is likely to describe clearly the behavior of the hydrocyclone so various empirical models has been introduced with various geometry and operating conditions.

The performance of the hydrocyclone depends strongly by the short circuiting to underflow and this is determined by the volumetric flow split between overflow and underflow defined as ratio of underflow volume flow rate to overflow volume flow rate.

The earliest model of hydrocyclone is was proposed by (Dahlstrom, 1949, 1951) uniform large diameter cyclone data, and gave a empirical equation for cut-size (Eqn 2.2)as,

$$d_{50a} = \frac{3 \times 10^3 (D_o D_i)^{0.68}}{Q^{0.53} (\rho_s - \rho_i)^{0.5}} \quad (2.2)$$

Followed by this (Bardley, 1965) proposed model for cut size (Eqn 2.3), assuming the laminar flow regime and considering the equilibrium orbit theory as,

$$d_{50a} = \frac{3 \times 0.38^n D_i^2}{k} \left[\frac{\mu_{sl}(1-R_f)}{D_c Q (\rho_s - \rho_l)} \tan\left(\frac{\theta}{2}\right) \right]^{0.5} \quad (2.3)$$

Both of the above equation, was developed from dilute slurries. These can be barely used for the complex flows and highly dense slurries, so the use of above models is very limited.

Based on experimental data of (Rao's, 1966) with a 50.8 cm diameter hydrocyclone (Plitt, 1976) has given models for flow split (Eqn 2.4) as,

$$S = \frac{a \left(\frac{D_u}{D_o}\right) (D_u^2 + D_o^2) h^d \exp(0.54\varphi)}{D_c^f H^g} \quad (2.4)$$

Where,

S represents volumetric flow split, D_u - Underflow Diameter, D_o : Overflow Diameter, D_c : Cylindrical Diameter, L_c : Length of cylindrical portion, H: Slurry feed head, H: Vortex finder to spigot distance, φ : Volume fraction of solids in feed, a, b, c, d, f, g – Empirical constants.

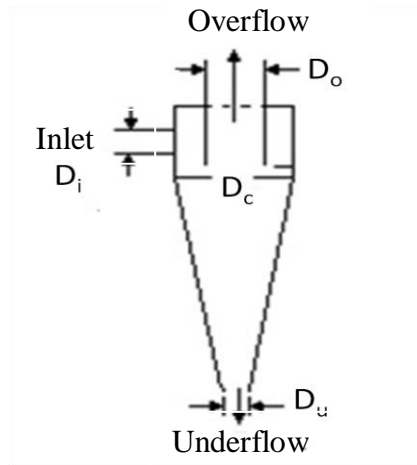


Figure 2.1: Dimensional details of hydrocyclone

Figure 2.1, shows the dimensional nomenclature of a hydrocyclone. The details for this are given in the chapters ahead.

And the cut size, d_{50} has given as, (Eqn 2.5),

$$d_{50} = \frac{aD_c^b D_i^c D_o^d \exp [6.3 \varphi]}{D_u^f h^g Q^i (\rho_s - \rho_f)^{0.5}} \quad (2.5)$$

Where, Q is flow rate of slurry.

Unlike Bradley and Dahlstrom, Plitt model was found more appropriately fitting for the experimental data's. However it is seen that different coefficients are required for the perfect fit while considering the industrial problems.

(Lynch and Rao, 1975) developed model for the corrected cut size(Eqn 2.6) using data from 10.2, 15.2, 25.4 and 38.1 cm krebs cyclones treating feeds of different size distributions (coarse, medium and fines):

$$\log(d_{50c}) = K_1 D_o - K_2 D_u + K_3 D_i + K_4 D_i - K_5 Q + K_6 \quad (2.6)$$

Where K_i ($i=1..6$) are positive constants significantly dependent on feed size distribution. (Nageswararao, 1978), proposed dimensionless d_{50} model (Eqn 2.7) using data from 10.2, 15.2, 25.4 and 38.1 cm diameter kreb's hydrocyclones including data's from (Rao's 1966) to as shown:

$$\frac{d_{50}}{D_c} = K_{dl} \left(\frac{D_o}{D_c}\right)^{0.52} \left(\frac{D_u}{D_c}\right)^{-0.47} \lambda^{0.93} \left(\frac{P}{\rho p g D_c}\right)^{-0.22} \left(\frac{D_i}{D_c}\right)^{-0.5} \left(\frac{L_c}{D_c}\right)^{0.2} \theta^{0.15} \quad (2.7)$$

Where $\lambda = \frac{C_v}{(1-C_v)^3}$;

C_v is volumetric fraction of solid in feed slurry (%).

K_{dl} depends on feed characteristics like feed distribution, specific gravity and Cyclone diameter give $K_{dl} = K_{do} D_c^{-0.65}$ as and P is Pressure. This was successfully fed as a model in JKMRC for industrial problem simulations. But it was observed that it could not give a good prediction above 30% of solid fraction. Also, it had a limitation that the cut-size at 0% solid fraction is zero, which was later on overcome by (Castro, 1990) and proposed new model for β instead of λ .

(Svarovsky, 1984) suggested the models (Eqn 2.8, 2.9, 2.10) using the dimensionless groups like Reynolds, stoke's and Euler number, including all the flow properties,

dimensions and separation process of hydrocyclone. The relations proposed are as follows,

$$Stk_{50} \cdot Eu = 0.0474 \left[\ln \left(\frac{1}{R_f} \right) \right]^{0.742} \exp (8.96 C_v) \quad (2.8)$$

$$Eu = 71Re^{0.116} \left(\frac{D_i}{D_c} \right)^{-1.3} \exp (-2.12C_v) \quad (2.9)$$

$$R_f = 1218 \left(\frac{D_u}{D_c} \right)^{4.75} Eu^{-0.3} \quad (2.10)$$

This is claimed to be scaled up till an increase of 10% by volume. Since these models are based on physical model, Svarovsky claimed that it will fit the practical experimental data fairly.

(Asomah, 1996) investigated and found the angle of inclination to be a factor for the performance of hydrocyclone. Whereas (Xiao, 1997), found that models give better predictions when the coefficients were refitted.

Lately, (Nageswararao, 2004), revised and noted that the 1978 model has a dimensional inhomogeneity. The constant K_{dl} was replaced by K_{pl} as (Eqn 2.11),

$$K'_{pl} = K'_{p0} \left(\frac{D_c}{D_{c,std}} \right)^s \quad (2.11)$$

The combined effect of feed material and non quantified variables now reflects the model constants for the standard cyclone, say K_{p0} . The relation between the new material constant, K'_{p0}

And the current K_{p0} could be expressed (Eqn 2.12) as:

$$K'_{pl} = K'_{p0} (D_{c,std})^s \quad (2.12)$$

2.1.1 Model Limitations: Though many such kind of model has successfully incorporated to understand the phenomenon, but the Nageswararao's model found not suitable for feed densities less than 30% and is only based on single average density models. In real life the minerals are always present in mixture form having different size and densities. If we consider coal, the mineral density (Firth, 1984) is widely distributed and the assumption of average particle density may lead to wrong results causing increased re-circulating loads to grinding mills. So there is need to study the influence of different components on performance of hydrocyclone. This gives us a motivation to proceed for the multicomponent studies.

2.2 Multicomponent separation concepts and Models:

The behavior of multi-component particles in a hydrocyclone is poorly understood and unaccounted for in most of the mathematical model equations available in the literature (Narasimha et al., 2012). The challenges have been seen in classification of the UG2 platinum circuits due to the difference in density between silica and chromites, the two major components of the ore (Mainza et al., 2004). Silica, the PGM carrying component, has an average density of 2.7 and chromites component has an average density of 4.5. They compared the performance of the conventional flat bottomed and three product cyclone by conducting tests under similar conditions. From their work it has been observed that chromites has lower cut-size than silica, indicating that large quantity of chromites reporting to underflow at a particular size, at which it is expected to escape through overflow. This results in loss of capacity for fresh feed and loss of energy by over grinding. They observed that size by size assays are required in quantifying performance of cyclone in the UG2 circuits.

(Kawatra, 2006), studied the inflection in hydrocyclone efficiency curves using mixture of quartz and magnetite. They observed the interference of particle separation due to the wake formation and agglomeration. The low density materials are seen dominating the overall efficiency curve at the coarser size and high density materials at the finer sizes. The inflection indicates that high density materials preferentially retained in grinding circuit and are being over ground.

(Mainza, 2006), studied the classification behavior of UG2 platinum ore in hydrocyclones. During the classification, the coarse silicates report to the overflow and the fine chromites to the underflow. The shape of efficiency-curve for overall classification of solids is observed different than normal. The classification curves for high density component (Chromite) and low density component (Silica) oriented at very fine solids and very coarse solids respectively. They observed that Individual density component follow standard shape for efficiency curves with low density component displaying fish-hook nature. So they realized that the classification can be modeled by considering individual density fractions.

(Weller et al., 1988), tried to develop a multi-component model for grinding and classification circuits. They used copper ore including copper, pyrite and gangue for their study.

(Narasimha et al., 2010), developed the concept of multi component particle classification. The authors have developed better empirical hydrocyclone model for hydrocyclone assuming average particle density. The new relationships were developed for water split, cut size and alpha. The model involves density function, which allows extending of the work for multicomponent particle. The Mathematical equations are:

The water split equation (Eqn 2.3):

$$R_f = K_w \left(\frac{D_o}{D_u}\right)^{-1.06787} \left(\frac{D_u}{D_c}\right)^{2.2062} \left(\frac{V_t^2}{R_{max}g}\right)^{-0.20472} \left(\frac{1}{\tan\left(\frac{\theta}{2}\right)}\right)^{0.829} \left(\frac{\mu_m}{\mu_w}\right)^{-0.7118}$$

$$\left(\frac{L_c}{D_c}\right)^{2.424} \left(\frac{V_h}{V_t}\right)^{-0.8843} \left(\frac{(\rho_s - \rho_f)}{\rho_f}\right)^{0.523} \left(\cos\left(\frac{i}{2}\right)\right)^{1.793}$$

(2.13)

Where,

K_w is constant depends on feed property, V_h and V_t represents hindered and tangential velocity, i as cone angle, μ_m / μ_w : viscosity of mixture / water.

The d_{50c} equation given by (Eqn 2.14):

$$\frac{d_{50}}{D_c} = K_{dl} \left(\frac{D_o}{D_c}\right)^{1.093} \left(\frac{D_u}{D_c}\right)^{-1.0} \left(\frac{(1 - f_v)^2}{10^{1.92} f_v}\right)^{-0.703} Re^{-0.936} \left(\frac{D_i}{D_c}\right)^{-0.936} \left(\frac{L_c}{D_c}\right)^{0.187}$$

$$\left(\frac{1}{\tan(\theta)}\right)^{-0.1988} \left(\frac{(\rho_s - \rho_f)}{\rho_f}\right)^{0.217} \left(\cos\left(\frac{i}{2}\right)\right)^{-1.034}$$

(2.14)

Where,

f_v : solid fraction of slurry and Re represents Reynolds No

The alpha equation as (Eqn 2.15):

$$\alpha = K_{ag} \frac{\left(\frac{D_o}{D_c}\right)^{0.27} \left(\frac{V_t^2}{R_{max}g}\right)^{0.016} \left(\cos\left(\frac{i}{180}\right)\right)^{0.868} \left(\frac{(1-f_v)^2}{10^{1.82}f_v}\right)^{-0.72}}{\left(\frac{D_u}{D_c}\right)^{0.567} \left(\frac{(\rho_s - \rho_f)}{\rho_f}\right)^{1.887} \left(\frac{\mu_m}{\mu_w}\right)^{0.127} \left(\frac{1}{\tan(\theta/2)}\right)^{0.182} \left(\frac{L_c}{D_c}\right)^{0.187}} \pi r^2 \quad (2.15)$$

The density function in above equations extended to multicomponent classification. The modified reduced cut-size equation (Eqn 2.16) for multi-component system is :

$$\frac{d_{50}}{D_c} = K_{dl} \left(\frac{D_o}{D_c}\right)^{1.093} \left(\frac{D_u}{D_c}\right)^{-1.0} \left(\frac{(1-f_v)^2}{10^{1.92}f_v}\right)^{-0.703} Re^{-0.936} \left(\frac{D_i}{D_c}\right)^{-0.936} \left(\frac{L_c}{D_c}\right)^{0.187} \left(\frac{1}{\tan(\theta)}\right)^{-0.1988} \left(\frac{(\rho_s - \rho_f)}{\rho_f}\right)^{-1.37} \left(\cos\left(\frac{i}{2}\right)\right)^{-1.034} \quad (2.16)$$

Some experimental part has been done to understand the hydrocyclone behavior in presence of magnetite and quartz in different proportion (Narasimha et al., 2014). In this study the interaction factor has been introduced, which we are trying to understand in better way in this study by various simulations.

2.3 Iron ore beneficiation

The huge demand of the iron ore for iron and steel industries have forced the tailing ponds level to higher level causing environmental and mineral loss issues. Various studies has been done to get appropriate technique for the beneficiation and utilizing this fraction in the sinter feed up to 40% by micro-balling of the sinter mix prior to sintering (Srivastava et al., 2000). Efforts were made to reduce alumina in the ore fines primarily focused on flocculation techniques (Mahiuddin, 1989). Some studies indicated that alumina and silica could be reduced to 3.5% and 1.4% respectively using the hydrocyclone based on the density difference (Mohanty, 2010) followed by Wet High Intensity Magnetic Separator (WHIMS). Experimental work is also available to reduce the alumina content of iron ore slime to 1.17% with a yield of 37% using hydro cyclone followed by spiral concentrator. But there was no better understanding of the phenomenon of the multicomponent behavior has been taken care in all of these. In this

study with the iron ore we are trying to explore the multicomponent behavior when the iron ore slimes are treated in hydrocyclone and make it more efficient.

2.4 CFD modeling for the hydrocyclones

The dominant behavior of hydrocyclone is the swirling flow nature. For solving this classical problem of hydrocyclone various turbulence models have to be used. In this study we are trying to solve the hydromechanics of 2inch and 3inch hydrocyclone with magnetite and quartz slurry using Computation Fluid Dynamics approach. The flow governing equations and turbulence models are solved simultaneously to get the flow pattern.

2.4.1 Turbulence

The high centrifugal force acting inside a hydrocyclone creates a high swirling flow and Reynolds number values usually is in the range of 10^5 to 10^6 (Bradley, 1965). With the high turbulent nature of flow hydrocyclone have a tendency to form air core in the axis of it, which is a result of pressure difference inside hydrocyclone and atmospheric pressure.

(Hinze, 1975), defined turbulence as “Turbulence fluid motion is an irregular condition of flow in which various quantities show a random variation with time and space coordinates so that statistical distinct average values can be discerned”

(Wilcox, 1994), explained the continuous spectrum of scales that varies from smallest to largest over several order of magnitude. He stated “A turbulent eddy can be thought of as local swirling motion whose characteristics dimension is the local turbulence scale.” He describes the transfer of the kinetic energy transfer from the large eddies to the smaller one.

(Davailles et al., 2012), studied the physics on hydrocyclone in a dilute flow medium using Eulerian multi-fluid modeling approach for fluid–particle with RSM turbulent flow modeling. Good estimate of cut size (d_{50c}) and reduced prediction of classification efficiency was observed at high concentrations high turbulent action and under prediction of the properties like viscosity etc in hydrocyclone. RSM model does not simulate the fluctuating velocity components accurately with an inherent equilibrium

turbulence assumption; it was able to predict reasonable velocity profiles with low computation power.

While simulating for the 10 phases, the particle also have great impact in form the extra swirls due to its separations process. In cases of high energy and momentum transfer of turbulent flows associates with large eddies coupled with small eddies. LES (large eddy simulation) coupled with VOF / ASM will give as more accurate estimation in highly complicated system, but in cost of high computational power.

(Narasimha et al., 2006), studied the flow of air and water phases through laboratory 75mm and 101mm hydrocyclones simulations. It is concluded that LES turbulence model led to an improved turbulence field prediction and thereby to more accurate pressure and velocity fields, Figure 2.2 .

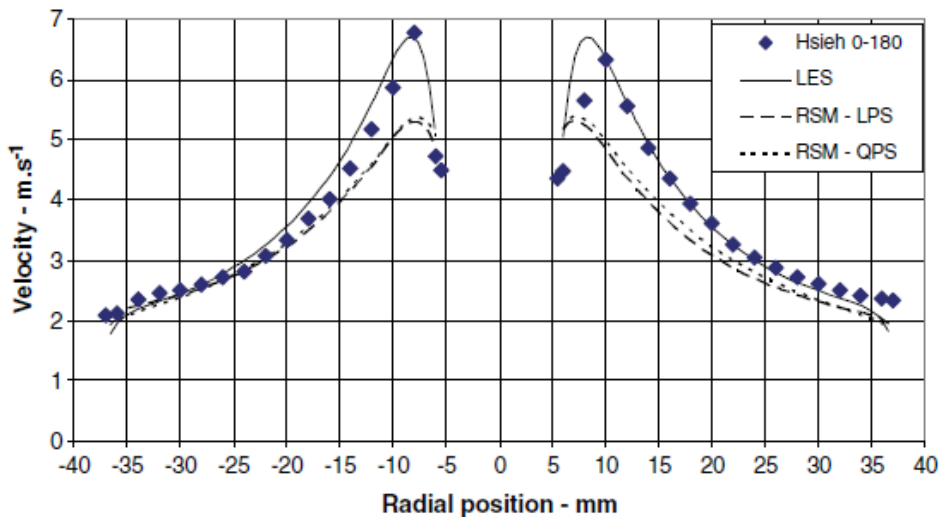


Figure 2.2: Comparison of predicted tangential velocities with experimental results for the 75mm hydrocyclone at 60mm from the roof of the cyclone wall (Narasimha 2006)

2.4.2 Multiphase model

Multiphase flows can be solved by a number of CFD techniques. For hydrocyclone air core formation it is important to choose and solve the interphase data's. Eulerian multiphase CFD approaches solve for the velocities and concentrations of the dispersed phases using transport equations and range in complexity from full Eulerian granular flow techniques, which solve the equations of motions for both dispersed and continuous phases to simplified approaches, such as the Mixture model (Manninen et al., 1996). VOF model (Hirt et al., 1981) uses two or more immiscible fluids by solving a single set

of momentum equations and tracking the volume fraction of each of the fluids through the domain.

The particulate phase flow dynamics can be solved using two approaches, Lagrangian and Eulerian. In very dilute phases, each particle tracking can be possible using the Lagrangian approach. When the number of phases increases and interaction between the phases are significantly it is easily solved using Eulerian approach, where a set of continuity, momentum and turbulence equation is solved for each phase. It can capture the fluid-solid and solid- solid interactions efficiently.

The Lagrangian method usually tracks transiently a large amount of particles. The method starts from solving the transient momentum equation (Eqn 2.17) for each particle:

$$\frac{du_p}{dt} = F_D(u - u_p) + \frac{g(\rho - \rho_p)}{\rho_p} + \bar{F}_a \quad (2.17)$$

The left hand side of the equation represents the inertial force per unit mass (m/s^2), where u_p is the particle velocity vector. The first term on the right hand side of equation is the drag term, where F_D is the inverse of relaxation time (s^{-1}) and u_G the air velocity; the second term represents the gravity and the buoyancy, where ρ and ρ_p are the density of the air and the particles, respectively; and \bar{F}_a stands for additional forces (per unit mass) that may be important.

The mixture model is derived from the full Eulerian multiphase transport equations by making two simplifying assumptions: (i) that the dispersed phases are moving at their terminal slip velocity relative to the continuous fluid phase and (ii) the interphase momentum transfer can be formulated by a simple drag calculation. Assumption (i) obviates the need to solve separate momentum equations for each phase in the system.

The Eulerian approach innately involves averaging of some sort, which implies more modeling. However the computational requirements of the Lagrangian approach scale directly with the number of particles, whereas the computational requirements of the Eulerian approach only scale with the number of resolved phases.

The Eulerian approach (Manninen et al., 1996) used to model multiphase flows based on the phases moving at different velocities, but assume local equilibrium over short spatial length scales. The advantage of the Lagrangian multiphase approach is that particle–particle and particle–fluid interactions are calculated dynamically for every particle

present in the system based on the instantaneous velocity of the particle (Narasimha et al., 2007). By comparison the Eulerian approach only calculates a phase velocity, a phase volume fraction and overall stresses associated with the average behavior of an ensemble of phase particles in a finite volume CFD grid.

Table 2-1: Summary of CFD modeling in hydrocyclone

Authors	Models	Dimensional Detail	Remarks
Boysan et al. (1982)	An algebraic turbulence model with non-vanishing angular component	2D	Model restricted to gas cyclone. Unable to predict an air-core
Davidson (1988, 1995)	Based on multi-continuum approach, without particle inertial forces	2D	Model for hydrocyclone without an air core
Hsieh and Rajamani (1988, 1991)	Prandtl mixing model with two turbulence scales. Extended Lagrangian approach to calculated particle trajectories	2D	Limited to low-solids concentrations
Dyakowski and Williams (1993)	Anisotropic character of turbulence	2D	The effect of mean velocity on turbulence. All six components of Reynolds stress. Limited only to hydrodynamics
Malhotra et al. (1994)	Used the k- ϵ model	2D	The new formulation of turbulence energy dissipation
Dyakowski and Williams (1995)	Calculation based on the internal pressure distribution	2D	The air-core diameter as the function of various hydrocyclone geometries and operational conditions
Slack and Boysan-1998	Used the RSM model for 3D simulation	3D	Result described by the velocity distributions

Ma et al. (2000)	Used the RNG model	3D	Particle tracking technique used for modeling particle motion
Slack et al. (2000)	LES with DPM	3D	Required a very fine mesh and long computational time.
Schuetz et al. (2003)	Used the RSM model with DPM	3D	Simulated separation efficiency curve. Limited to low solid concentrations.
Cullivans et al.(2003)	RSM model with quadratic pressure strain	3D	Accurate prediction of air-core
Narasimha et al. (2006)	RSM, LES coupled with VOF model	3D	Air core modeling and diameter prediction
Wang et al.(2007)	RSM and VOF model	3D	Air core modeling
Brennan et al.(2007)	Multiphase Modelling - ASM	3D	Predict classification and distribution of limestone using fluent. Explained the short circuiting flow concept.
Kuang et al. (2012)	RSM and ASM model with modified drag and viscosity models.	3D	Estimated coal particle hydrocyclone classification performance
Davailles et al. (2012)	RSM and DPM model	3D	Feed solids concentration distribution
Narasimha et al. (2012)	Mixture model with modified lift forces and viscosity model	3D	Particle segregation inside Renner's hydrocyclone

Chapter 3

Methodology

The multicomponent study in hydrocyclone classification has been attempted in this thesis, by considering pure bicomponent and naturally occurring ore, including multi components. Artificial mixtures were subjected for classification to get the hydrocyclone performance. Subsequently, Iron ore slime mainly containing three components were considered for the detail studies of naturally occurring ores and its beneficiations. In the following chapter the designs, operating parameter and procedures are described in detail.

3.1 Bi-component Experiment Methodology:

The bi-component experiments are carried with two materials Magnetite and silica. Where the magnetite size is varying from -150 to 2 microns and silica from -200 to 0.5 microns having density of 4950 kg/m³ and 2650 kg/m³ respectively.

The experiments were carried out in 2 inch hydrocyclone with a wide range of combination w.r.t operating parameters as mentioned in Table 3-1.

Table 3-1: Design of Experiment for 2inch Hydrocyclone

Solid %	Vortex finder	Spigot	Proportions
5	11, 14	3.2,4.5,6.4	1:9, 2:8, 1:1, 8:2, 9:1
10	11, 14	3.2,4.5,6.4	1:9, 2:8, 1:1, 8:2, 9:1

The total experiments as total with full factorial makes 60 numbers. In this study we have only considered 32 experiments, i.e 2 extra after being fractionally factorising by half factorisation design method and optimizing the experiment combinations, reducing the alias experiments. Figure 3.1 shows the combinations of the experiments attempted.

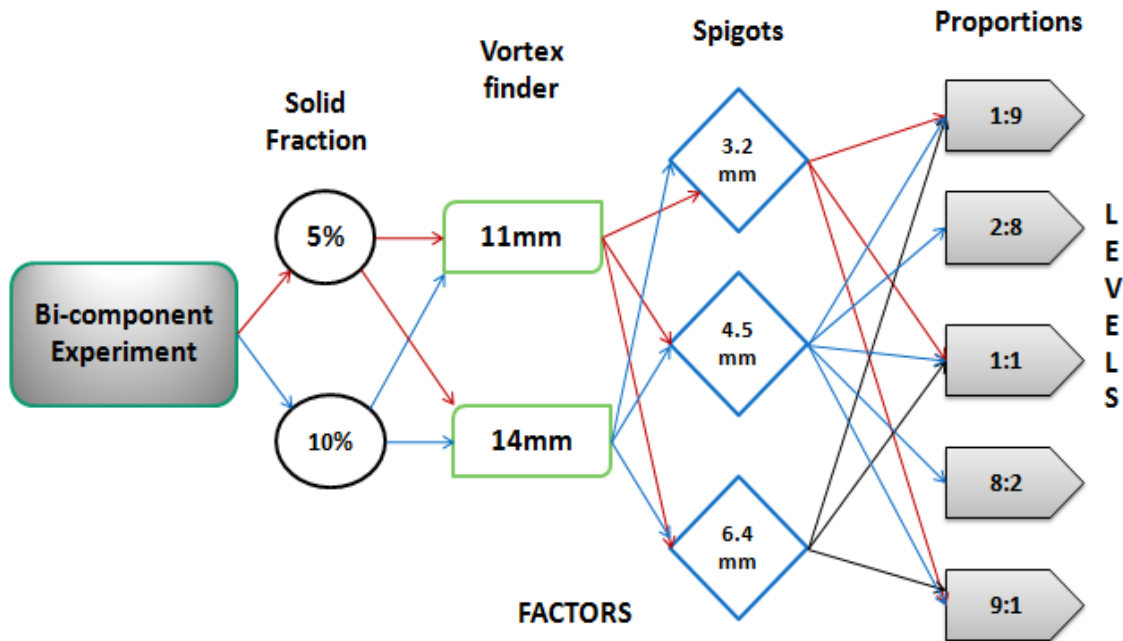


Figure 3.1: Design of experiment for 2 inch hydrocyclone - Bicomponent studies

Sample Preparation and Hydrocyclone test

The magnetite and silica were mixed in the above mentioned proportion in 30 liters water by weight percent. At a constant pressure of 110 KPa (1.1 bar). After starting the experiment wait for 2 mins to attain a steady state. The overflow and underflow were then collected for 5 sec in containers, weighed for the flow rate measurement and the same recorded for three repeats.

Two set sample 'A' and 'B' of sample were collected from the inlet and outlet of hydrocyclone. Sample 'A' was subjected to solid fraction of the streams by drying in oven. The before and after drying weighs provides us data for the solid % calculation.

Sample 'B', is taken for the separation of the magnetite and silica thereby analysis of respective the particle size distribution. The 'B' sample subjected to devis tube and also hand-magnet to separate out the components.

All the data consolidated and subjected to mass balance for both solids and water overall mass balance of system, which provides solid recovery (R_s), water split (R_f). Component overall mass balance yeilds solids recoveries component wise, similiarly size wise produces the mass recovered to underflow, which represents classification (efficiency) curve for overall mixture and component wise also.

The same concepts were taken to work with naturally occurring ore i.e. Iron ore which is as described in section 3.2.

3.2 Iron Ore Slime Experiment Methodology:

The iron ore slime is collected from NMDC, brought from Dalli's Bhilai steel plant fine stack having a size range from -235 to +37 microns. This slimes are consisting the main components as Iron around 50%, Alumina 5.2%, and silica as 18% in average. Since we want to understand the behavior of the multidensity materials in a hydrocyclone during the classification, it is very appropriate sample to go with. Since all the three component have different densities and also content in various sizes also varies as shown in Table 3.2

Table 3-2: Iron ore slime compositions

Iron ore Slime			
	Fe ₂ O ₃	Al ₂ O ₃	SiO ₂
Densities (g/cc)	5.24	3.95	2.7
Microns	%	%	%
235	49.8	4.24	19.56
149	56.8	2.66	13.6
100	55.6	2.68	15.08
74	52.2	2.71	19.8
50	50	3.13	23.1
44	50.2	3.05	22.8
37	50.6	3.03	21.14
-37	39.6	20.04	13.83

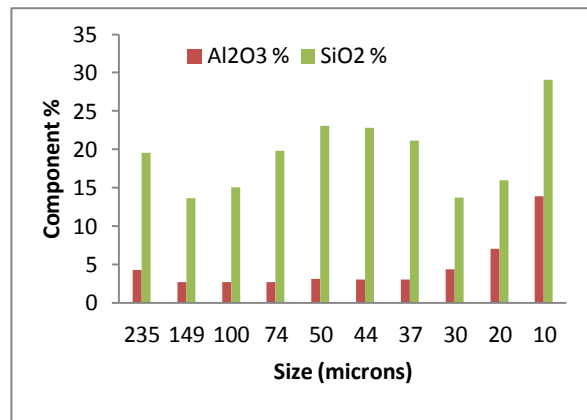


Figure 3.2: Alumina and silica distributions

From Figure 3.22 we observed that the alumina content in the iron ore as majority present below -54 micron and for further understanding of the multicomponent we have consider only the -54 microns for analysis from the total output stream samples rejecting +54 micron particles. The SEM EDx average and spot wise analysis is shown in Figure 3.33. The analysis gave qualitative component distribution information in the feed in various size fractions. The analysed values could not able produce accurate data

as it is single surface scanned data. The idea of the distribution of major components is then further analyzed by ICP.

ICP – Induced Coupled Plasma

The iron ore sample digested to liquid sample by microwave digester at 200⁰C for 45 mins including heating and cooling. The sample is diluted to ppm level using 5% HNO₃ and got subjected to the ICP for the analysis.

XRF – X Ray Diffraction

The very fine powdered material subjected under the X-Ray fluorescence. Multi-element analysis of iron ore provides the overall concentrations of the main constituents of the product, but does not give any indication of the identity of chemical phases present which we can have seen a glimpse in the Scanning Electron Microscopy(SEM) – EDx.

The experimental studies though gives a good prediction in individual experiments for d₅₀ and R_s but the number of experiments were not sufficient to give strong evidence about the multicomponent interaction. Hence the computation fluid dynamics studies has been taken for different combinations of the magnetite and silica.

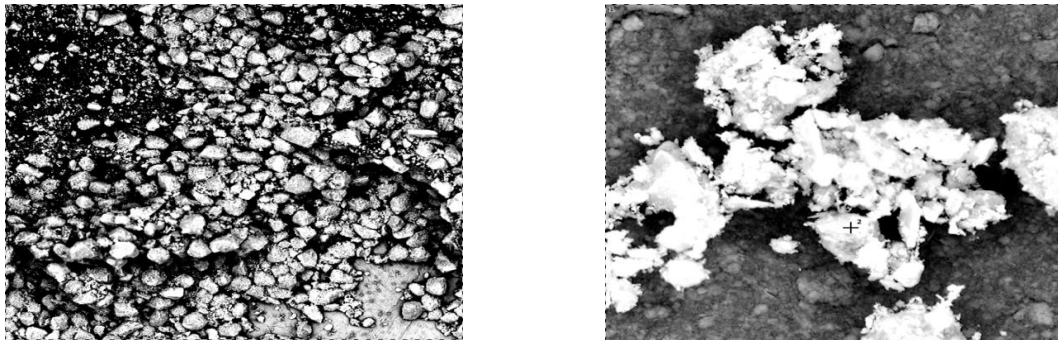
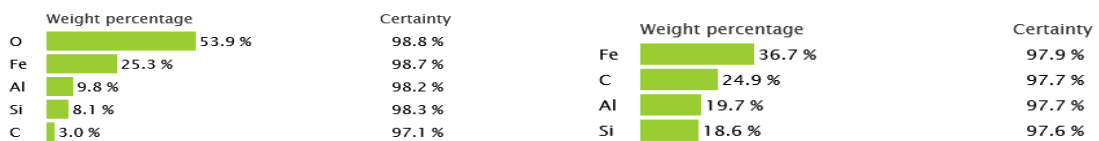


Figure 3.3: 1.Avarage analysis (-34) and 2. Spot analysis (+54) - SEM



3.2.1 Hydrocyclone Test Rig for Iron ore experiment

The experiments are carried out in 4 inch hydrocyclone test rig . Both water only and slurry experiments were taken out with a feed percent of 15 % solids are run. Each measurement has been made triplicate to reduce the errors. The samples from underflow and overflow of cyclone are collected simultaneously for genuine particle size

distribution change. The collected slurries then dried and measured the weight to get the weight %.

As most of the Alumina reported was under -54 micron shown in Figure 3.2, hence for further studies each sample that is feed , underflow and overflow under 54 microns subjected for sizing in 5 different fractions using cyclosizer with -10, -20, -30, -40, -50 micron size to understand the distribution of the the components size wise. Component analysis by chemical and ICP taken out for each of the size fractions for the prediction of the performance of hydrocyclone with various designs.

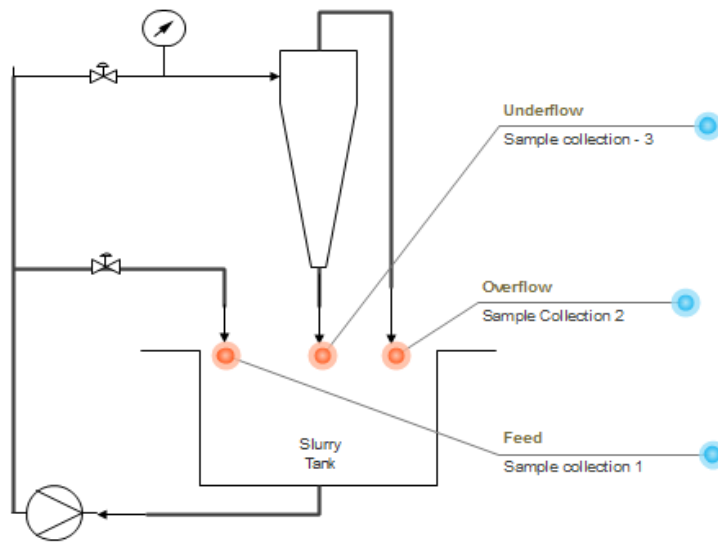


Figure 3.4: Schematic Diagram: Experimental set up of Hydrocyclone

3.2.2 Hydrocyclone Experiments

Table 3-3 shows the combinations of the 4 inch hydrocyclone experiment carried out:

Table 3-3: Design of experiments - 4 inch hydrocyclone

Test No	Designs	solid %	Pressure (Psi)	Vortex finder(mm)	spigot (mm)
1	WR-CC	15	10	14	17.5
2	WR-CC	15	10	14	15
3	WR-CC	15	10	14	25
4	WR	15	10	14	17.5
5	WR	15	10	14	15
6	R	15	10	14	25

Where , WR-CC : Without Rod cone change

WR – Without Rod

R – With Rod

3.2.3 Size wise Characterization Approach

Chemical Analysis of Iron using potassium Dichromate

Solutions and Chemicals Required:

Dried sample, standard $K_2Cr_2O_7$, concentrated HCl, $SnCl_2$ solution, $HgCl_2$ solution, H_3PO_4 , diphenylamine sulfonate indicator.

Sample Preparation :

Take dried sample into 250 ml flask. conc HCl to the flask. Heat the solution to just below boiling on the hot plate until the ore dissolves.

Heat each solution containing the iron sample almost to boiling. Carefully add $SnCl_2$ solution drop wise until the yellow Fe (III) colour just disappears. Then add 2 drops excess of $SnCl_2$ solution. Cool the flask to below $40^\circ C$. Add 10ml of $HgCl_2$ solution. A small quantity of a white precipitate should appear. If no precipitate forms or if the precipitate is grey or black, the trial must be discarded. Wait for some time. Add 5ml of concentrated sulphuric acid and 7ml of syrupy phosphoric acid. Dilute with distilled water to bring the volume to about 125ml. Cool the solution to room temperature. Add 8 drops of barium diphenylamine sulfonate indicator and slowly titrate with your standard $K_2Cr_2O_7$ solution from a blue-green, through a greyish tinge to the first permanent violet, which is the end point. The titration should be conducted drop wise.

Chemical Analysis of Alumina using EDTA

Sample preparation:

Take 0.5 gm sample, add fusion mixture (sodium carbonate + potassium carbonate) and fuse it at $1000^\circ C$ in a platinum crucible for around 40 minutes. Cool till room temperature.

Wash the fused sample in a beaker using 1:1 Hcl solution from the platinum crucible; again wash properly with distilled water. Heat stlightly and make up the solution to 250ml with warm water.

Alumina tests EDTA method

The Iron in the sample.

From the 250 ml sample prepared take 25ml in conical flask, add sulfo cylicic acid Indicator (1 spatula) it will turn to red wine color. Add ammonium hydroxide(1:6) drop wise till it gives yellow color. Add 1:10 HCl drop wise again it will turn to red wine color, with one drop extra of it. Titrate with 0.01 M EDTA till will turn to colorless.

Determination of alumina through EDTA Method

Add 15 ml excess EDTA solution to the same 250 ml conical flask from burette after titrating iron oxide. Add 1 ml phosphoric acid (1:3) and 5 ml of sulphuric acid (1:3) and one drop of thymol blue (light pink) in to the titration flask. Add ammonium acetate solution by stirring until the colour changes from red to (yellow). Add 25 ml ammonium acetate in excess to obtain pH approximately 5.5 to 6.0. Heat the solution to boiling for one minutes and the cool. Add 50 mg of solid xylenol orange indicator(yellow) and titrate with bismuth nitrate(pink to brick red-note the point) solution slowly with stirring until the colour of the solution changes from yellow to red. Add 2 to 3 ml of bismuth nitrate solution in excess. Titrate with 0.01 M EDTA solution to a (sharp yellow- note) end point from red colour.

The percentage of alumina in the sample is calculated as given in Eqn 3.1,

1 ml of 0.01 M EDTA = 0.5098 mg Fe₂O₃,

Alumina oxide (Al₂O₃), % = 0.5098 x (V/W)

$$V = V1 - V2 - (V3 \times E) \quad (3.1)$$

Where,

V = volume of EDTA for alumina in ml;

V1 = total volume of EDTA used in the titration in ml;

V2 = volume of EDTA used for iron in ml;

V3 = total volume of bismuth nitrate solution used in the titration in ml

W = weight of sample in gm;

E = equivalence of 1 ml of bismuth nitrate solution.

Equivalence of bismuth nitrate solution is obtained as follows-

Transfer 100 ml of bismuth nitrate solution to a 500 ml conical flask and dilute with about 100 ml distilled water. Add a few drops of thymol blue solution and ammonium acetate solution until the colour changes from red to yellow. Add 50 mg of xylenol orange indicator and titrate with 0.01 M EDTA solution until the colour changes from red to yellow. The equivalence (ml of EDTA) of 1 ml of bismuth nitrate solution is calculated as follows.

$$E = V_4/W_1$$

Where, V_4 = volume of EDTA solution in ml.

W_1 = volume of bismuth nitrate solution in ml

3.3 CFD Methodology

The data from bi-component experiments at 10% solids are taken as the base for the computational studies and model understanding. The Simulations are done in 3 inch hydrocyclone for the primary interactions. 2 inch hydrocyclone simulation have been tested for feasibility. It has yet to be established in full form.

3.3.1 Cyclone geometry and grid generation

The cyclone dimensional details that has taken for simulations are shown in table 3-4:

Table 3-4 : 3 inch and 2 inch Cyclone dimensions

Parameters	Dimensions (in mm)	
Cylindrical diameter D_c	76.2	44.5
Conical length	400	308
Cylindrical length	150	123
Inlet	45(circular)	11 x 5(square)
Overflow Diameter	32	14
Spigot Diameter	12.5	4.5

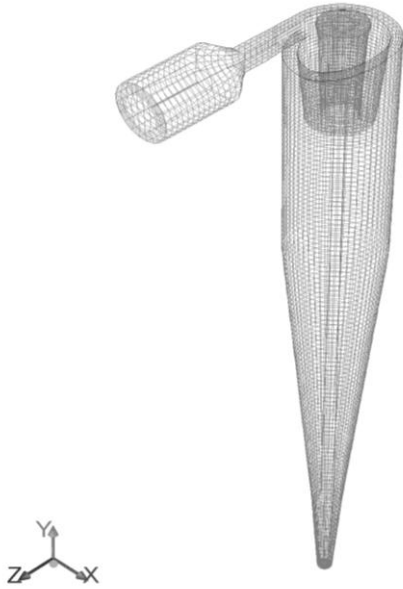


Figure 3.5: 3inch Hydrocyclone Mesh



Figure 3.6: 2 inch Hydrocyclone Mesh

The pressure drop and recovery to underflow as a function feed water flow rate was measured experimentally and compared with Simulated datas.

The 3 dimensional body geometry was fitted grids (Figure 3.5 and 3.6) were generated in ICEM and encompassed the flow space from the feed port to the underflow and the top of the vortex finder. The approach used was identical to that reported (Brennan et al., 2009).

3.3.2 Boundary condition :

The feed port is velocity inlet boundary condition and the overflow and underflow were pressure outlet boundary conditions. All other boundary conditions were wall boundaries. An extensive range of grids were generated for the cyclone geometries but only a subsection are reported .

3.3.3 CFD Modeling

The problem was solved using Fluent 14.0. Using Reynolds Stress model(RSM) for and LES for 2 inch and 3inch hydrocyclones for the turbulence modeling, Aircore generation by Volume of fluid (VOF) model and Mixture model for the multiphase development.

Flow Governing Equation:

The numerical treatment of the Navier–Stokes equations is the backbone of any CFD technique. Navier–Stokes incompressible equations supplemented by a suitable turbulence model are appropriate for modeling the flow in hydrocyclone.

The continuity equation, assuming incompressible flow with no mass source terms is given as (Eqn 3.2) (Wilcox, 1994):

$$\frac{\partial u_i}{\partial x_i} = 0 \quad (3.2)$$

Where, u_i is representing velocity components and x_i as the distance in i -direction. The momentum equation for the incompressible flow in non accelerating reference form may be represented by Navier stoke's equation (Eqn 3.3) as:

$$\rho \frac{\partial u_i}{\partial t} + \rho u_i \frac{du_i}{dx_j} = -\frac{\partial P}{\partial x_i} + \frac{\partial \tau_{ij}}{\partial x_j} \quad (3.3)$$

Where, P represents pressure, ρ as density, u_i velocity components in i^{th} directions ($i=1,2,3$ as x, y and z direction respectively), t is time and τ_{ij} is known as viscous stress tensor defined by Eqn 3.4,

$$\tau_{ij} = 2\mu S_{ij} \quad (3.4)$$

μ = Molecular viscosity, S_{ij} = strain rate tensor as Eqn 3.5

$$S_{ij} = \frac{1}{2} \left(\frac{\partial u_i}{\partial x_j} + \frac{\partial u_j}{\partial x_i} \right) \quad (3.5)$$

Turbulence :

Reynolds (1895) introduced a procedure where the instantaneous quantities are expressed in terms of summation of mean and fluctuating components (Figure 3.7). And

given as

$$u_i = u_i' + U_i$$

where u_i : instantaneous velocity

u_i' : fluctuation velocity

U_i : mean velocity

The figure below is representing a combination of mean and fluctuating velocities ,

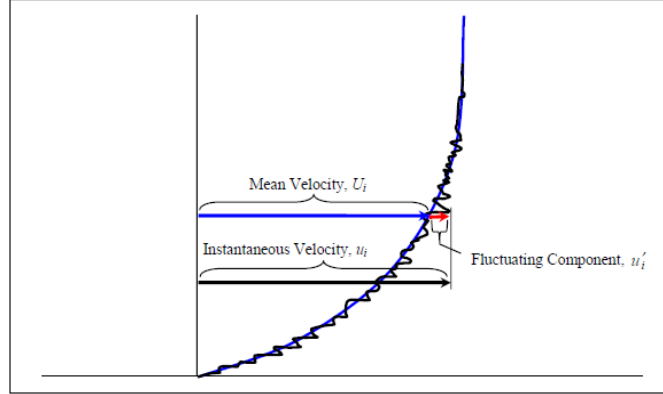


Figure 3.7: Mean and fluctuating velocity

Reynold's Stress Model:

Time averaging the Navier stoke's equation in conservative form, is shown as Eqn 3.6 (Wilcox, 1994).

$$\rho \frac{\partial U_i}{\partial t} + \rho u_i \frac{d(U_i U_j + \overline{u_i' u_j'})}{dx_j} = - \frac{\partial P}{\partial x_i} + \frac{\partial (2\mu S_{ji})}{\partial x_j} \quad (3.6)$$

Where , U_i, U_j, S_{ij}, P represents the mean values and the symbols u_i['] and u_j['] represents the fluctuating velocities. The appearance of term $\overline{u_i' u_j'}$ is a statistical correlation that resulted from the time averaging method which, in general is not equal to zero and which represents the mean value of the product of velocity fluctuations, which are produced due to the turbulence effects in the flow. The purpose of turbulence modeling is to define this term and has tried in various ways.

The transportation equations used to solve is defined as Eqn 3.7,

$$\frac{\partial(\rho \overline{u_i' u_j'})}{\partial x} + \frac{\partial(\rho u_k \overline{u_i' u_j'})}{\partial x_k} = D_{T,ij} + D_{L,ij} + P_{ij} + \Phi_{ij} + \epsilon_{ij} + F_{ij} \quad (3.7)$$

Where, the two terms in the LHS are the local time derivative of the stress and convective transportation term, respectively. And D_{L,ij} is molecular viscous diffusion

term; P_{ij} is stress production term; F_{ij} is rotation production term. The remaining items were as follows:

The turbulent diffusion term:

$$D_{ij}^T = \frac{\partial}{\partial x_k} \left(\frac{\mu_t}{\sigma_k} \frac{\partial \overline{u'_i u'_j}}{\partial x_k} \right) \quad (3.8)$$

The pressure strain term:

$$\Phi_{ij} = -C_1 \rho \frac{\epsilon}{k} \left(\overline{u'_i u'_j} - \frac{2}{3} k \delta_{ij} \right) - C_2 \left(P_{ij} - \frac{2}{3} p \delta_{ij} \right) \quad (3.9)$$

The dissipation term:

$$\epsilon_{ij} = -\frac{2}{3} \delta_{ij} \rho \epsilon \quad (3.10)$$

Where C_1 and C_2 were constants, k is turbulent kinetic energy, ϵ is turbulent dissipation rate, and μ_t is turbulent viscosity coefficient. These constitute the basic governing equations of a three dimensional turbulent flow problem. Since the RSM accounts for the effects of streamline curvature, swirl, rotation, and rapid changes in strain rate in a more rigorous manner, it has a greater potential to accurately predict complex flows, as in the case of hydrocyclone.

Large Eddy Simulation (LES)

In LES the larger scales of turbulence are resolved by the equations of motion and scales which are smaller than the grid modeled. Thus the equations of motion are filtered and the result is that an additional stress tensor appears in the filtered Navier Stokes equations which accounts for the transfer of momentum by sub grid scales of turbulence. The sub grid scale (SGS) stresses are usually modeled (Eqn 3.11) using a simple eddy viscosity:

$$\tau_{ij}^{sgs} = -\mu_{sgs} \left(\frac{\partial \overline{u}_i}{\partial x_j} + \frac{\partial \overline{u}_j}{\partial x_i} \right) \quad (3.11)$$

In this work the Fluent implementation of the Smagorinsky Lilly SGS (Smagorinsky, 1963) model is used. This model proposes that the SGS eddy viscosity is related to the local average grid spacing and the mean strain rate.

The turbulent stresses in the tensor τ_{ij} were calculated using (a) the RSM (Launder et al, 1975) with the Launder Linear pressure strain model and quadratic pressure strain model

and also (b) LES using the standard Smagorinsky-Lilly sub grid scale model with a default $C_s=0.1$ (Smagorinsky, 1963).

Volume of Fluid and Mixture Model:

The hydrocyclone generates air-core at its axial position, which behaves stability concern at time while changing the input operating conditions. So it is very important to consider the air-core formation as very precisely to get a good simulated flow field. For the same we incorporate the multiphase model in solving hydrodynamics of hydrocyclone. These two models are embedded in fluent solver, and have similar approach for solving the interfaces, where the mixture models have an additional drift velocity calculation. In recent studies these are used to solve the air-core solution.

The tracking of the interface between the phases is accomplished by the solution of a continuity equation for the volume fraction of one of the phases. For q^{th} phase, the equation shown as Eqn 3.12:

$$\frac{1}{\rho_q} \left[\frac{\partial(\alpha_q \rho_q)}{\partial t} + \nabla \cdot (\alpha_q \rho_q v_q) \right] = S_{\alpha_q} + \sum (m_{pq} - m_{qp}) \quad (3.12)$$

Where \dot{m}_{qp} the mass transfer from phase q to phase p and \dot{m}_{pq} is the mass transfer from p to q phase. The volume fraction equation is solved based upon the secondary phase.

The VOF model is used for solving the water air combination where there is a free surface between two immiscible continuous fluid phases and to resolve the air core. The primary phase was treated as water and the secondary phase was treated as air. The VOF model solves a transport equation for the air phase concentration (Eqn 3.13):

$$\frac{\partial \alpha_p}{\partial t} + \frac{\partial(\alpha_p u_{mi})}{\partial x_i} = 0 \quad (3.13)$$

Whereas the mixture model solves the equations of motion for the fluid mixture and transport equations for the volume fractions of any additional dispersed phases (Eqn 3.14)

$$\frac{\partial}{\partial t} \alpha_k + \nabla \cdot (\alpha_k u_m) + \nabla \cdot (\alpha_k u_{km}) = 0 \quad (3.14)$$

$$u_{km} = u_k - u_m \quad (3.15)$$

The u_{km} is the drift velocity (Eqn 3.16) of the phase k with respect to the mixture and is calculated from the slip velocities of the other dispersed phases:

$$u_{km} = u_{kc} - \sum_{l=1}^n \frac{\alpha_l \rho_l}{\rho_m} u_{lc} \quad (3.16)$$

u_{kc} is the slip velocity of the dispersed phase k relative to the continuous fluid phase c and is calculated from the equilibrium drag assumption. A number of previous studies have conducted the experimental and simulation data validations. (Raziyeh et al., 2014) have done experiments with industrial scale cyclones using copper as a component and at various solid fractions and operating parameters, the results were well validated with respect to the experiments.

The simulations started with laminar flow at rated flow was with each cyclone. The equations were solved using the unsteady segregated solver with a time step of 5×10^{-4} s.

The following discretization preference were used in this work :

SIMPLE for pressure velocity coupling, PRESTO for pressure and QUICK for the VOF equation. The momentum equations used QUICK with the RSM simulations and Bounded Central Differencing with LES. The numerical approach was to start with the cyclone domain “full of water” and at a base flow rate and integrate in time until the swirl created a axial region of negative pressure. At this point the backflow volume fraction of air at the overflow and underflow was set to 1 and the simulation proceeded so that air was drawn in to form the air core.

The simulation then conducted till steady mass flow rates out the overflow and underflow and a steady feed pressure were obtained.

Chapter 4

Experimental - Results and Discussions

Overall

The experiments discussed above are mass balanced and analyzed size and component wise. Sizing of the sample is done by physical sieves and cycloizer, later on subjecting it to chemical, ICP and XRF analysis for the estimation of composition. For bicomponent studies since the magnetite is easily separable by magnetic separations, treated by hand magnet and devis tube as mentioned in methodology, chapter 3. The analysed data is summarised in Table 4.1 .The detailed bi-component cassification data, although based on small size cyclone is pretty much important to understand the basic phenomenon of the particle behaviour under various operating conditions.

Following are the details of the results and noteworthy outcomes

4.1 Bi component (silica and magnetite) hydrocyclone experiments.

4.1.1 Experiments with feed slurry:

A. Effect of Feed pressure on throughput

The Figure 4.1 nad 4.2 shows the effect of feed pressure on throughput of hydrocyclone.

It is observed that the throughput increases with feed pressure as observed in literatures

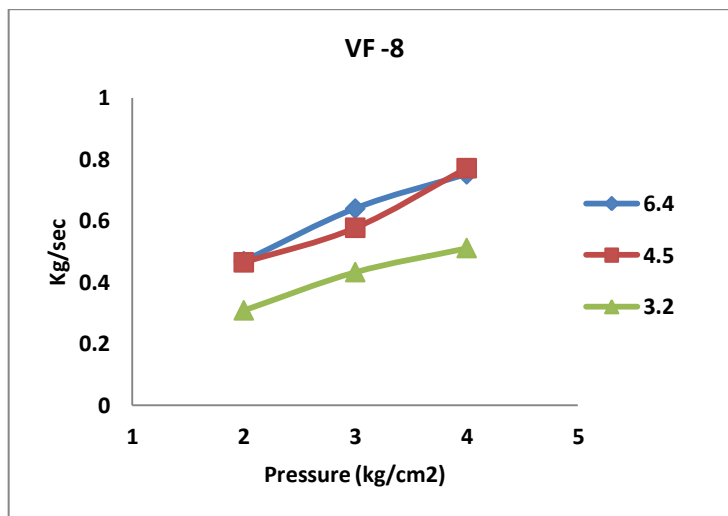


Figure 4.1: Flow rate Vs Pressure variation (2 inch -8VF)

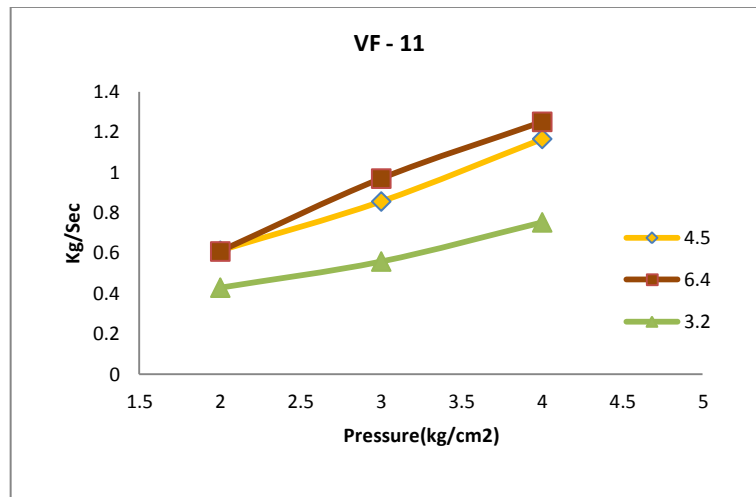


Figure 4.2: Flow rate Vs pressure variation (2 inch-11 VF)

It is observed that the total flow increases as the spigot size increases. At the same time when the vortex finder size increases from 8mm to 11mm the flow specifically to overflow increases.

The detailed calculation for the hydrocyclone experiment is set below:

B. Flow Rate Determination for Experiments:

Duration of sample collection = 5s

Weight of underflow collected, trial 1=0.34 kg

Weight of underflow collected, trial 2=0.33 kg

Weight of underflow collected, trial 3=0.33 kg

Underflow flow rate, average = 0.0653 kg/s

Overflow flow rate, average =0.202 kg/s

Feed Flow rate =0.266 kg/s

C. Determination of dry solid percentage in sample:

Weight of underflow sample=160 g

Weight of dried sample =77 g

Percentage of dry solid = 48.13 %

The dry solid percentage in feed and overflow samples can also be calculated in the same approach.

C. Classification of samples by Magnetic Separation:

The sample is separated into components using a hand magnet and a devis tube separator repeatedly. It is observed that the magnetic separation is done with good accuracy.

Table 4-1: Summary of Experiments and Results - 2Inch hydrocyclone

REF	SOLID FRAC	Do	Du	PROP.	d50 (mix)	d50 (mag)	d50 (silica)	alpha (mix)	alpha (mag)	alpha (silica)	Rs (mix)	Rs (mag)	Rs (silica)	Rf
1	5	14	3.2	1:9	11.34	9.69	12.64	3.82	4.56	5.91	54.50	64.47	46.22	10.15
2	5	14	3.2	2:8	11.74	9.16	13.46	3.97	4.22	6.51	76.92	78.98	47.17	11.08
3	5	14	3.2	1:1	10.53	7.67	13.63	4.33	2.78	4.17	73.76	82.82	44.35	9.24
4	5	14	3.2	8:2	11.34	8.22	13.98	0.27	0.72	0.60	68.29	74.88	59.97	9.57
5	5	14	3.2	9:1	16.24	15.39	20.09	2.54	2.23	4.43	73.74	79.87	60.57	5.92
6	5	14	4.5	1:9	8.38	5.76	10.65	4.04	2.36	5.39	70.82	77.13	55.46	19.91
7	5	14	4.5	1:1	11.16	9.00	12.33	1.48	0.72	3.85	68.39	79.03	55.27	12.39
8	5	14	4.5	9:1	16.25	11.10	20.49	2.02	0.62	2.86	67.49	72.69	60.16	5.86
9	5	14	6.4	1:9	8.60	5.54	11.67	1.18	0.89	2.84	58.14	78.08	49.26	7.08
10	5	14	6.4	1:1	12.72	9.04	15.13	0.75	0.60	1.41	69.66	76.25	51.15	6.88
11	5	14	6.4	9:1	9.12	8.16	11.43	2.05	2.04	2.23	69.79	87.31	59.32	7.48
12	5	11	4.5	1:9	8.82	8.73	14.48	2.73	1.57	5.19	68.90	86.20	32.74	10.88
13	5	11	4.5	2:8	12.09	7.60	16.98	3.60	0.52	3.62	68.62	79.68	45.98	9.92
14	5	11	4.5	1:1	12.74	11.10	15.93	1.98	0.87	2.73	69.58	80.47	61.22	9.03
15	5	11	4.5	8:2	12.57	9.39	15.04	2.77	1.64	3.38	69.42	74.74	63.94	8.49
16	5	11	4.5	9:1	12.07	10.61	14.21	2.31	2.08	2.95	60.36	78.23	65.83	6.13
17	10	14	3.2	1:9	8.46	7.18	11.43	0.73	2.28	4.26	65.29	70.62	58.95	17.97
18	10	14	4.5	2:8	17.04	9.94	20.12	46.50	2.48	6.50	68.57	87.20	52.17	15.30
19	10	14	3.2	1:1	10.43	7.92	13.48	4.43	2.91	6.38	63.01	74.93	50.61	10.26
20	10	14	4.5	8:2	21.39	11.86	24.96	1.06	0.31	3.79	66.69	79.34	60.12	9.34
21	10	14	3.2	9:1	16.28	11.63	19.83	1.36	1.73	5.17	61.00	80.68	46.10	7.98
22	10	14	4.5	1:9	16.81	11.47	19.14	3.70	1.76	4.16	58.49	81.76	51.46	17.46
23	10	14	4.5	1:1	10.49	7.77	12.30	3.72	3.58	7.70	65.83	82.39	55.16	14.86
24	10	14	4.5	9:1	11.69	5.60	13.47	4.05	4.05	4.05	65.05	88.50	51.16	5.66
25	10	14	6.4	1:9	13.63	3.98	16.29	2.48	0.05	5.68	64.18	81.64	52.64	12.78
26	10	14	6.4	1:1	10.16	7.97	14.54	1.71	2.67	3.06	72.33	82.70	51.93	11.34
27	10	14	6.4	9:1	9.24	7.41	15.26	2.84	2.13	2.46	63.09	86.70	54.02	7.66
28	10	11	4.5	1:9	13.30	8.51	17.23	2.77	1.70	2.50	67.30	87.10	48.05	11.72
29	10	11	4.5	2:8	11.51	8.66	15.47	4.50	1.53	5.19	72.37	89.45	45.52	11.49
30	10	11	4.5	1:1	11.95	9.23	15.16	5.00	3.80	5.64	75.84	85.40	70.65	11.62
31	10	11	4.5	8:2	12.10	9.18	15.06	4.16	2.16	6.12	75.85	84.50	71.14	10.92
32	10	11	4.5	9:1	9.68	8.45	12.77	2.19	1.83	5.62	62.44	83.88	72.34	8.39

D. Size Analysis:

The separated and dried samples are subjected to size analysis by laser diffraction size analyzer. Size analysis for each sample is done thrice and average size distribution is used for efficiency calculations.

E. Solid recovery Calculations:

Underflow flow rate, $U=0.0653$ kg/s

Overflow flow rate, $O= 0.202$ kg/s

Feed flow rate, $F= 0.266$ kg/s

Solid fraction in underflow, $U_s= 0.4813$

Solid fraction in overflow, $O_s= 0.0156$

Solid fraction in feed, $F_s= 0.049$

Fraction of magnetite in underflow, $U_m=0.77$

Fraction of magnetite in overflow, $O_m=0.0673$

Fraction of magnetite in feed, $F_m=0.025$

$$\begin{aligned}\text{Recovery of solids, } R_s &= (U \cdot U_s) / (F \cdot F_s) \\ &= (0.0653 \cdot 0.4813) / (0.266 \cdot 0.049) \\ R_s &= 0.699\end{aligned}$$

$$\begin{aligned}\text{Recovery of Magnetite, } R_{sm} &= (U \cdot U_s \cdot U_m) / (F \cdot F_s \cdot F_m) \\ &= (0.0653 \cdot 0.4813 \cdot 0.77) / ((0.266 \cdot 0.049 \cdot 0.025) \cdot 100) \\ &= 0.7193\end{aligned}$$

$$\begin{aligned}\text{Recovery of Quartz, } R_{ss} &= R_s \cdot (1 - U_m) / (1 - F_m) \\ &= (0.699 \cdot (1 - 0.77)) / (1 - 0.025) \\ &= 0.5114\end{aligned}$$

$$\begin{aligned}\text{Water Split, } R_f &= (\text{water in underflow}) / (\text{water in feed}) \\ &= ((F_s - O_s) \cdot (100 - U_s)) / ((U_s - O_s) \cdot (100 - F_s))\end{aligned}$$

$$=0.06876$$

The Overall recovery, magnetite recovery and silica recovery calculated for each size fraction to determine efficiencies in same procedure.

F. Efficiency curve – detailed calculation:

$$\begin{aligned} \text{. Actual efficiency for quartz} &= (R_{ss} * d_{su}) / f(d) \text{ calculated} \\ &= (R_{ss} * d_{su}) / ((R_{ss} * d_{su}) + (1 - R_{ss}) * d_{so}) \\ &= (0.5114 * 3.32) / (0.5114 * 3.32 + (1 - 0.5114) * 7.77) \\ &= 0.3091 \end{aligned}$$

$$\text{Actual efficiency for magnetite} = 0.6804$$

$$\text{Actual overall efficiency} = 0.5131$$

$$\begin{aligned} \text{Corrected efficiency} &= (0.3091 - R_f) / (1 - R_f) \\ &= (0.3678 - 0.06876) / (1 - 0.06876) = 0.3091 \end{aligned}$$

From the series of data obtained, the size respective to 50 % efficiency is called as the cut-size.

$$d_{50\text{silica}} = 15 \mu\text{m.}$$

$$d_{50\text{magnetite}} = 9 \mu\text{m.}$$

$$d_{50\text{mixture}} = 12 \mu\text{m.}$$

For few experiments the procedure were repeated for twice to get the experimental precision check. Two of the experiments analysis compared are shown in figure 4.3 and figure 4.4. This shows the only variation come in the size distribution analysis where as rest of the calculations are under 2-5 % error.

It is also observed that the recovery with the slight change in solid % of feed effect a lot to the individual i.e. magnetite and silica solid recoveries to the underflow, for which it is very essential to take care of inlet feed % .

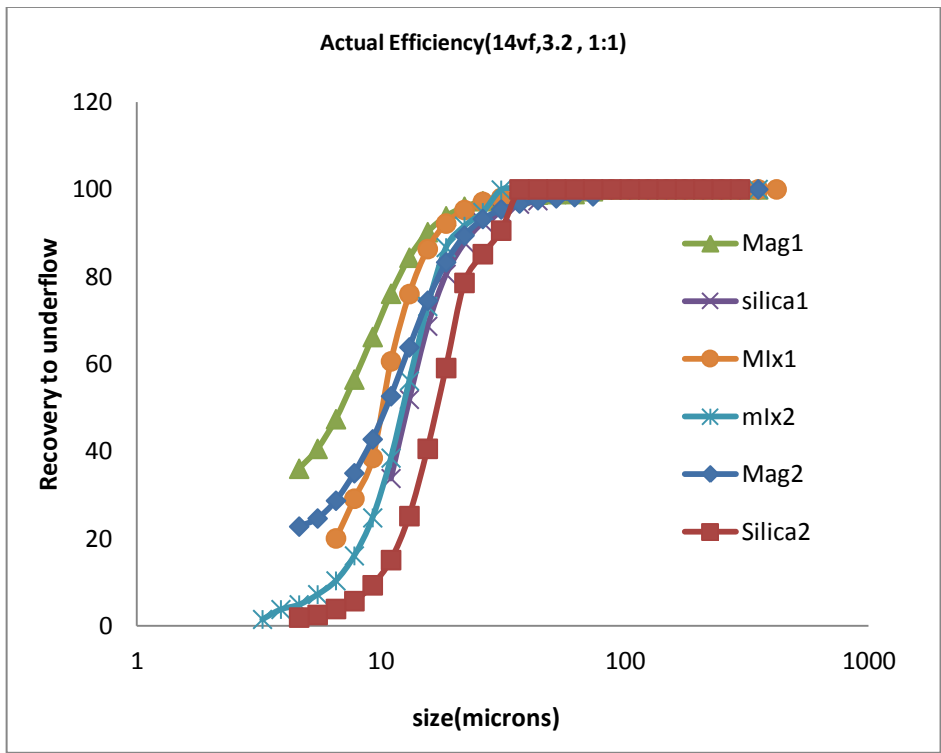


Figure 4.3: Actual efficiency curve - comparison of two experiments

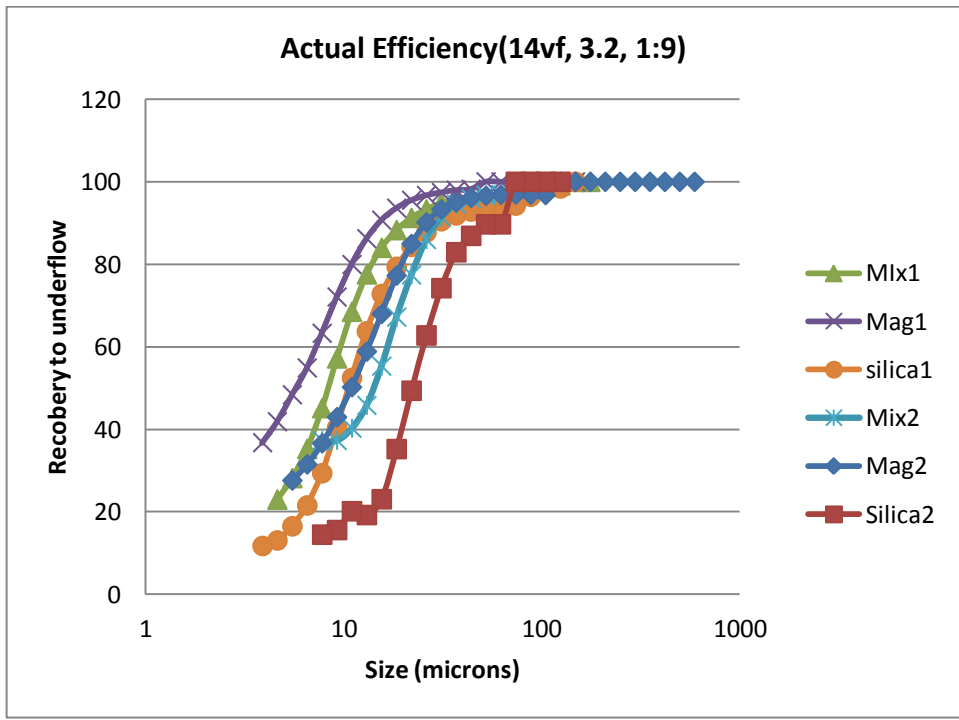


Figure 4.4: Actual efficiency curve - Comparison of two experiments

G. Cut-size variation with % of magnetite

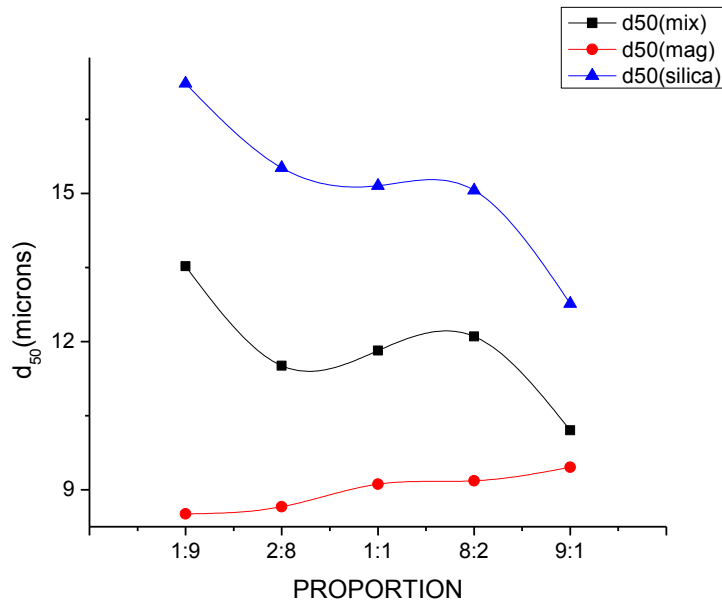


Figure 4.5 : d_{50} (At 10%) Vs Proportions

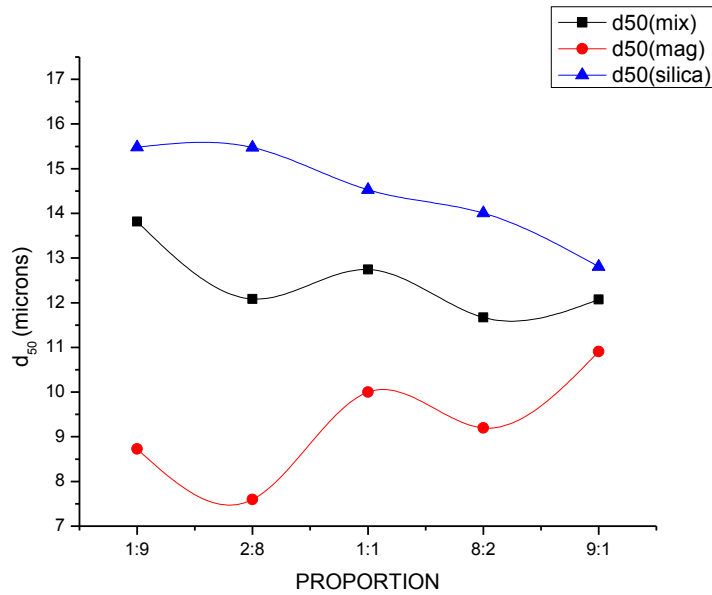


Figure 4.6: d_{50} (At 5%) Vs Proportions

In the above, Figure 4.5 and Figure 4.6, the d_{50} is been plotted against various composition with 5% and 10% solids respectively. Due to the high centrifugal action in hydrocyclone, and this force being a function of mass, the heavier particles tends to report towards the wall faster. Hence, the larger and high density particle is seen

reporting to underflow more and hence taking up a low d_{50} with respect to the lighter component. The mixture since having both components d_{50} (mix) lies in between the 2 components. In both cases with increase in % of magnetite it is observed that the d_{50} for magnetite increases and the d_{50} silica.

C. Cut-size variation with spigot diameter

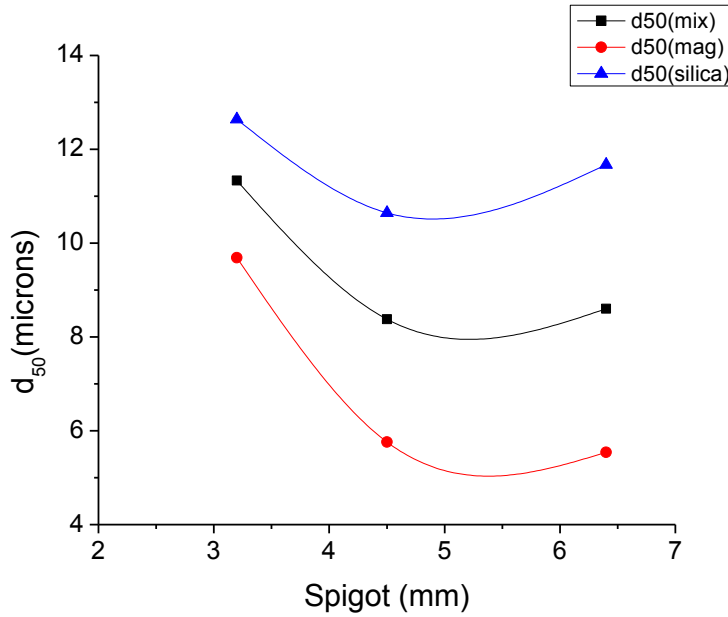


Figure 4.7: d_{50} Vs Spigots diameter (1:9) 5 % solids

In Figure 4.7, 4.8 and 4.9, the plots describe the component behavior as the spigot size increases. With the increase in the spigot opening the pressure difference inside hydrocyclone and atmosphere reduces and hence making the material flow easier to come out from it. At a constant vortex finder and increasing spigot diameter, there is comparatively high material loading towards underflow. As the spigot size increases which result to the solid % reporting to the underflow increases, the cut size of the components extracted from heterogenous mixtures decreases as compared to the pure components.

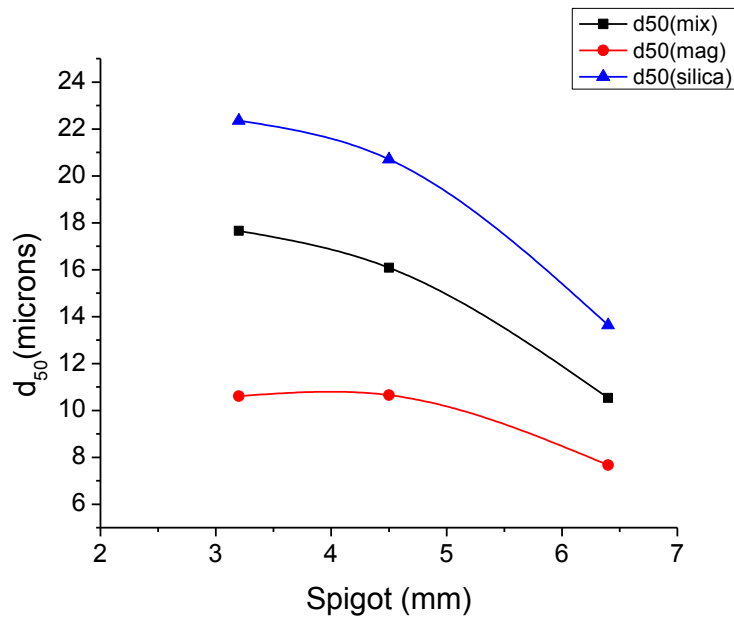


Figure 4.8 : d₅₀ Vs Spigots diameter (1:1) 5% solids

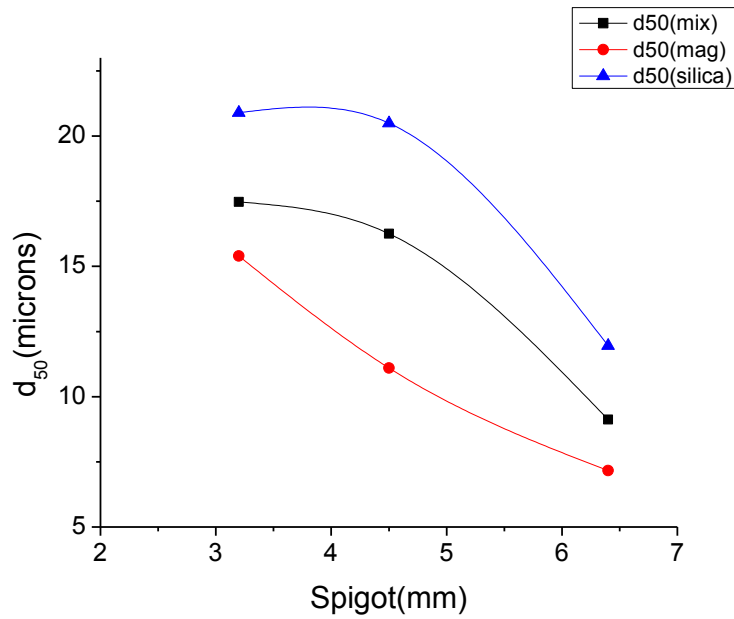


Figure 4.9 : d₅₀ Vs Spigots diameter (9:1) 5% solids

F. Cone force effect.

The hydrocyclone operations that employ in a non-transparent hydrocyclone it is difficult to locate the position of the LZVV; however, (Bradley, 1965) proposed estimation for the position of its base given below as:

$$R_{LZVV} = R_c \times \frac{R_o}{R_o + R_u}$$

Where R_o - the vortex finder radius R_c - the cyclone radius R_u - the spigot radius. Various studies aiming at evaluating the effect of the cone force ratio on the performance of a small diameter hydrocyclone, concluding the cut size decreases as the locus of zero vertical velocity (LZVV) shifts inwards has seen. Also the water recovery to the underflow observed increasing with an increase in the cone force ratio.

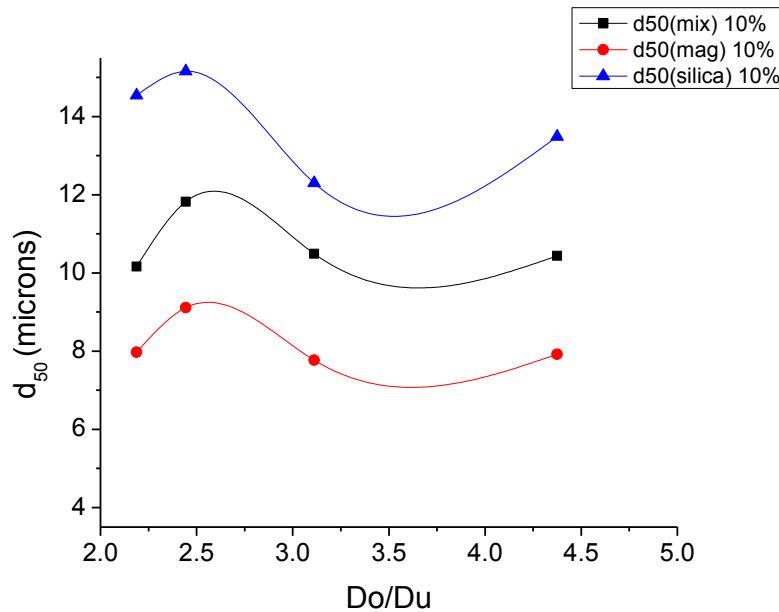


Figure 4.10: force ratio (Do/Du) effect on d50 (10% solids)

In Figure 4., the variation of d_{50} Vs cone force ratio from this experiment has analyzed at four different design parameters. The lower cut size, d_{50} indicates the maximum solid fraction reporting to underflow, and LZVV shifts towards the air-core.

G. Effect of Solid Recovery with Various Proportions

The high density particle having larger mass experience a larger centrifugal force and reports mainly to the underflow so as compared to silica the Rs of magnetite is higher. But there is little significant change with respect to the change in compositions. In silica the Rs increases with % magnetite increases, it could be the due to the engulfment of silica particles in the higher mass particle and reporting to the underflow. Figure 4.11 illustrates the argument appropriately.

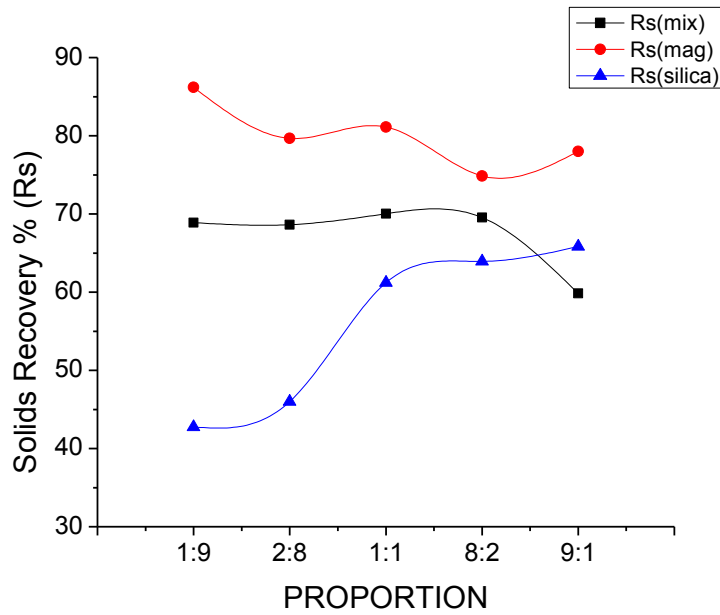


Figure 4.11: Rs Vs Component Composition

H. R_f at different designs parameters

As discussed earlier the solid as in total increases to underflow with the % of magnetite, also decreases the water reporting to the underflow. Due to the higher mass of magnetite, when the solid % increases in feed mixture, it tries to occupying the wall size at conical section. It is prominent because of sudden increase of the flow in conical section. When this phenomenon takes place the magnetite tries to push the water towards the air-core, hence maximum proportion of magnetite occupies the underflow reducing the water in underflow stream. From this we can also conclude that the fraction of components to the underflow has a direct effect of density. It leads to higher interference with the lighter component (silica) due to entrainment at higher % of heavier particle (magnetite). This can be clearly seen from Figure 4..

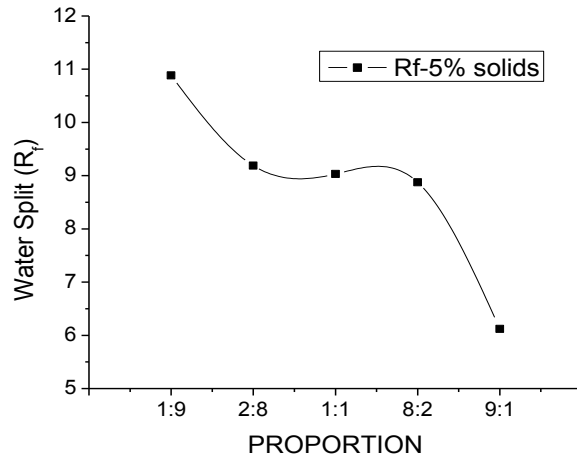


Figure 4.12 : R_f Vs Different Component compositions at 5% solids

I. Actual efficiency Curves

Analysis of the particle classification in hydrocyclone is represented by the actual efficiency curve shown Figure 4.1 and Figure 4.. These plot were extracted from size wise analysis considering the solid recovery and water split datas as mentioned in previous section. The cutsize and sharpness of separation were produced from the heterogenous mixture and compared with the pure form of components. The cut size of the pure component is found to be lower than the components when they are classified from the heterogenous mixtures.

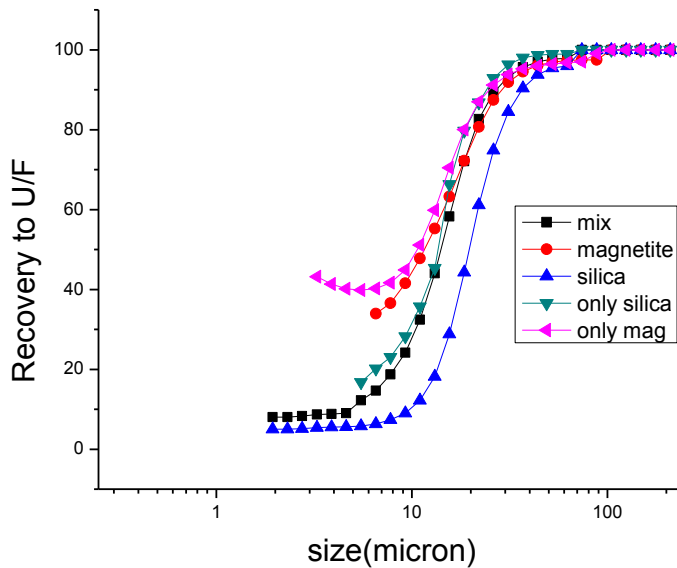


Figure 4.13: Actual efficiency curve: 10% solid, 1:1 (Magnetite:Silica)

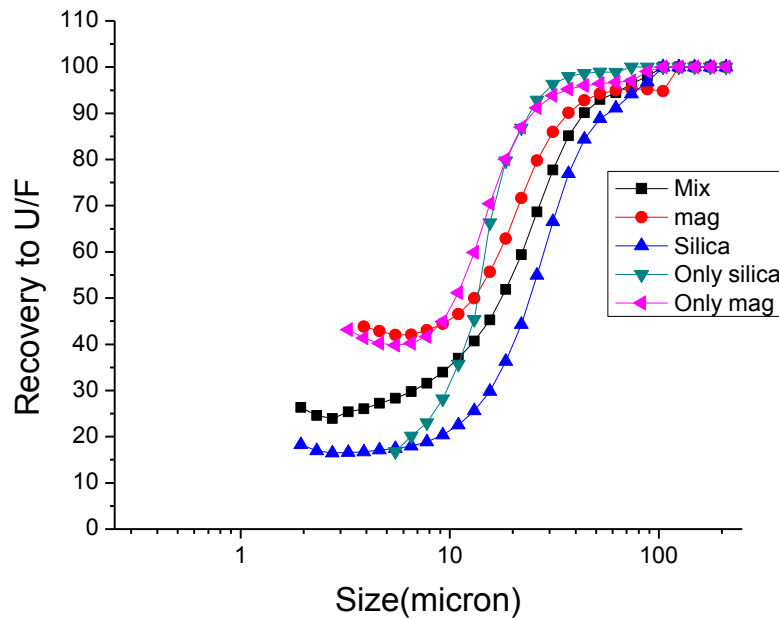


Figure 4.14: Actual Efficiency curve : 5% solid 1:1 (Magnetite:Silica)

Key observation taken from the efficiency curves are as follow:

- The efficiency curve of the overall mixture and the extracted silica and magnetite from the hetrogenous mixture shows less steeper than the pure components. That implies the reduction or deviation of the efficiency of mixture from ideal plot is much higher, reporting higher cutsize caused by the mixture.
- d_{50} – The silica and magnetite from the mixture give a higher d_{50} than the pure form because of the interference of particle in the complex flow and separationAs discussed in previous section.
- R_s and R_f : With increase in the % magnetite we can see the the magnetite reporting to underflow increases, Figure 4.and simultaneously the R_f i.e. water reporting to underflow decreases with % magnetite and % solids, Figure 4.
- Sharpness of separation: 2 inch hydrocyclone have high turbulance and less residence time for the material involved for classification the sharpness of separation varies very much. Magnetite being comparatively higher in density when being treated in 2inch hydrocyclone, easy escapes and shows lower sharpness of separation as compared to silica.

4.2 Iron ore slime Hydrocyclone experiments and Analysis

4.2.1 Silica Slurry experiments: Design selection

Ultrafine classification required large centrifugal forces, historically the typical size 2", 3" and 4" were adopted. (Thella et al., 2012) done study on processing of high alumina iron ore slimes using combination of 2" hydrocyclone classification and flotation, Dai et al (1999) have conducted experiments on solid - liquid two-phase flow studies in a 3" hydrocyclone. They predict very precise and reliable data's for the suitable flow depiction.

As the 4" has the maximum capacity among the aforementioned sizes we have selected 4" hydrocyclone as suitable experimental set up. In order to minimize the number of experiments with respect to iron ore slimes, initial test were conducted by using silica slurry.

The mentioned designs in **Error! Reference source not found.4-2** consists of tangential inlet, tapered vortex finder with two conical sections with angles of 12⁰ and 10⁰. Tapered vortex finder helps in increasing the residence time of coarse particles by enforcing into free vortex flow, thus reduce the short circuiting of coarse fraction to the overflow. The small cone angle reduces the amount of water split to the under flow, therefore high amounts of water results through the overflow leads to possibility of minimize fine fraction misplacement in the underflow.

Table 4-2: Design of experiments (Iron ore Slime)

Test No	Designs	Cone angle	Vortex finder (mm)	spigot (mm)
1	HC10	10	14	17.5
2	HC10	10	14	15
3	HC10	10	14	25
4	HC12	12	14	17.5
5	HC12	12	14	15

The above parameters were taken at 15% of solid fraction and 10 psi. The foremost plots shown in Figure 4. illustrates that the HC12_25 and HC10_15 shows a better performance than HC12_20.4, giving us a lower cut size and better separation curve. Hence the table 4-2 shows the combinations of the 4 inch hydrocyclone experiment carried out at 68.9 Kpa (10psi) and the initial overall analysis is specified.

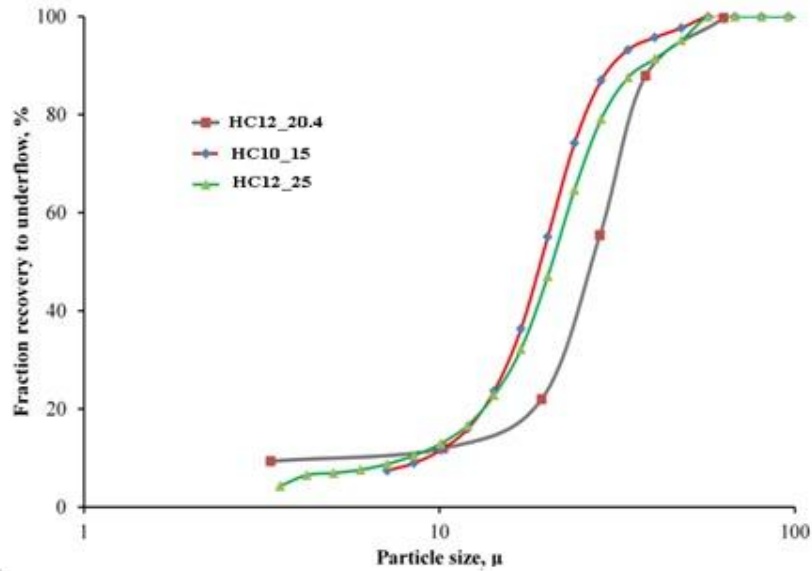


Figure 4.15: Silica slurry partition curve with different hydrocyclone designs

Increase in the pressure value leads to increase in flow rate, this causes increase in the air sucking and hence forming a larger air core. In this experiment the chosen optimum pressure i.e.10 Psi which shows relatively effective and stable air-core formation and better separation, which was observed by the spray discharge.

Table 4-3 : Solid % for 3inch Hydrocyclone (Iron ore slimes)

Experiment	Design	spigot		Sample(dried)	% solid
I	WR-CC	17.5	feed	87.7	16.03877
	WR-CC	17.5	UF	473.4	62.49505
	WR-CC	17.5	OF	18.2	2.115787
II	WR-CC	15	feed	115.8	19.25187
	WR-CC	15	UF	18.6	64.46547
	WR-CC	15	OF	320.2	2.215605
III	WR	17.5	feed	100.8	17.62238
	WR	17.5	UF	105.5	64.80745
	WR	17.5	OF	521.7	14.30702

IV	WR	15	feed	75.8	13.42306
	WR	15	UF	16.2	69.64711
	WR	15	OF	292.1	2.149396
V	WR	25	feed	132.4	20.47317
	WR	25	UF	15.4	38.35774
	WR	25	OF	233.1	1.896318

Where , WR – CC : Without rod and cone changed(10^0)

WR – Without Rod and old cone (12^0)

R – With rod and old cone (12^0)

Here we can remark that the maximum of ore concentration is going to underflow, including the iron ore in more percentage. Studies on the performance, water split and d_{50} for each component present in the ore were also done to get higher efficiency of the beneficiation process using hydrocyclones.

4.2.2 Water split

Water split ratio of the experiments has recorded to understand the performance of the ore and the hydrocyclone designs. It is also considered as to get the corrected efficiency curve for the experiment. The figure 4.16 shows the water split of overall, Iron and alumina with respect to various Designs of experiments taken:

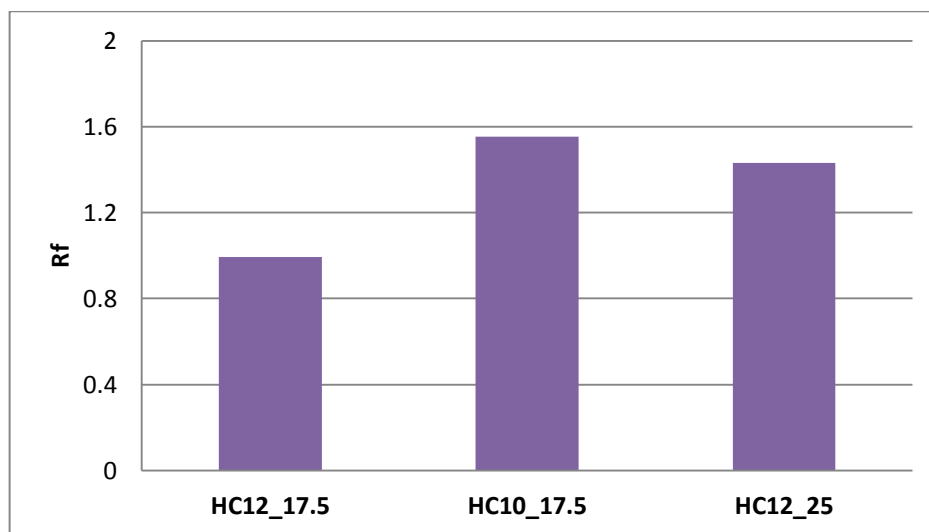


Figure 4.16: Water Split Vs DOEs

4.2.3 Solids recovery (Rs):

The solid recoveries to the underflow plot are shown as below:

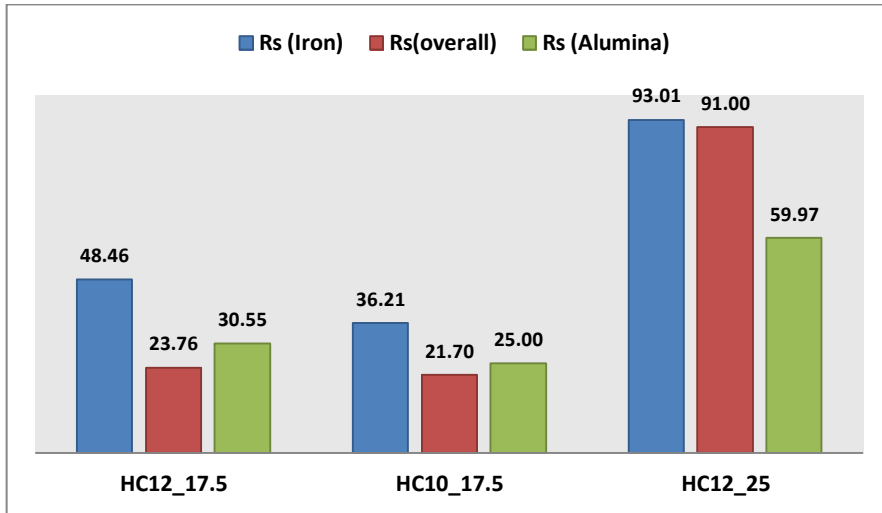


Figure 4.17: Solid Recovery Vs different Designs

The Figure 4. shows that there is a significant change for different spigots where as the change in cone is not that effective at same operating conditions. Among the three components as the iron have the highest density; the centrifugal force on it is higher as compared to the others which can be clearly seen from the d_{50} obtained in this figure. It is also observed that as the spigot size increases the water split and hence the solids reporting to underflow also significantly increases, because of the larger opening and easy release of the inside pressure, which has been also seen in case of bi-component studies.

4.2.4 Performance behavior of components:

Each of the component analysis has been done for the component wise performance monitoring. Table 4-4 shows the summary of the experiments performance data's. Following the same the resulted plots of the efficiency of 3 components at 5 different sizes has been illustrated.

Table 4-4: Performance parameters analyzed from Iron ore Slimes experiment

Performance parameters analyzed from Iron ore Slimes experiment

Sl no	Du	Rod	Cone Angle	Rf overall	Rs overall	Rs Iron	Rs Al ₂ O ₃	D50 overall	D50 Iron	D50 Al ₂ O ₃
1	17.5	N	12	0.994	23.75	48.4	30.55	21.5	14.5	30.5
2	17.5	N	10	1.553	21.70	36.2	25.00	21.5	14.5	30.5
3	25	N	12	1.432	91.00	93.0	59.96	19.2	16.3	38.6
4	25	Y	12	3.535	94.30	97.0	20.67	20.85	34.08	74.80

Figure 4.18, 4.19 and 4.20 shows the efficiency curves for each experiment. The effect of the multi-density behavior of various components present in the iron ore with different designs.

A. Actual Efficiency curves :

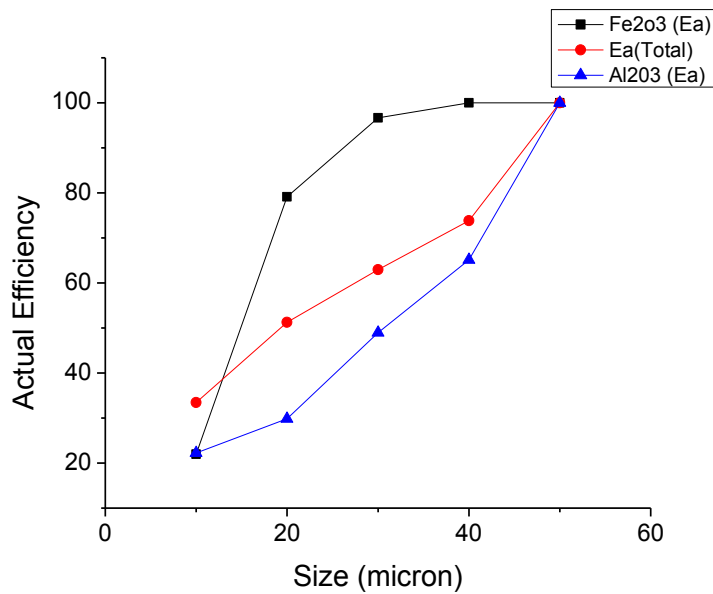


Figure 4.18: Tega hydrocyclone (spigot 17.5 / cone 12⁰)

B.

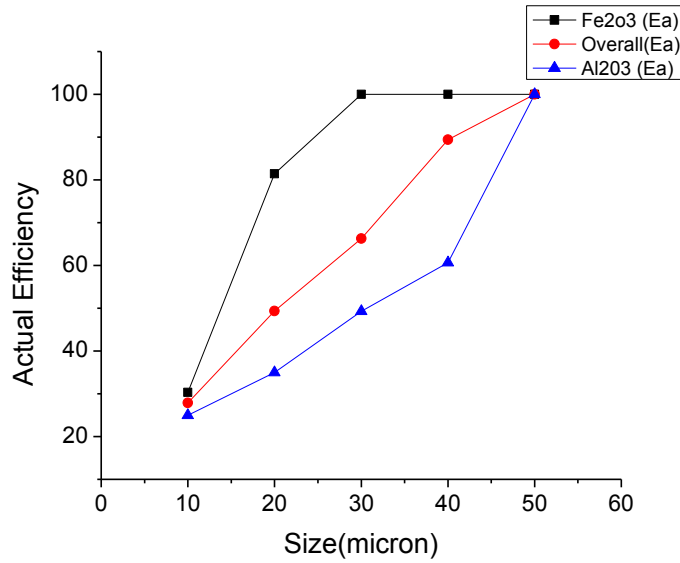


Figure 4.19: Tega hydrocyclone(spigot: 17.5/ cone: 10⁰)

It is observed that the high density component is having lower cut-size than light density component, whereas the overall mixture cut-size lies in between these, because of the high centrifugal force acting on the heavier particle that is iron reports mostly to the underflow easily. The Alumina content in the underflow is observed as around 3%.

C.

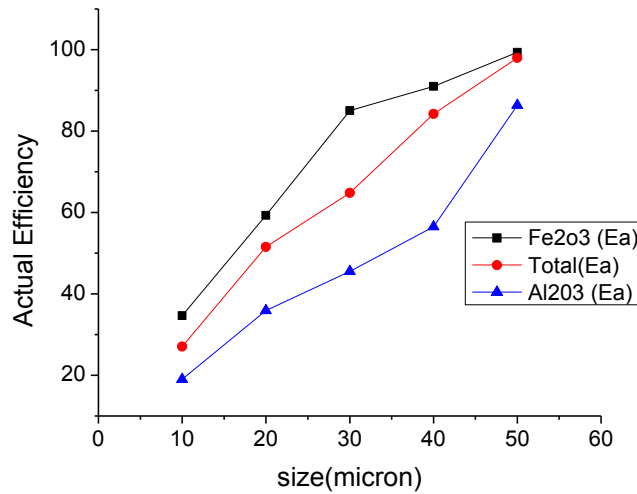


Figure 4.20: Tega hydrocyclone (spigot :25 / cone : 120)

The alumina collection changes with the change of the angle and the spigot size because the change in the hydrodynamic behaviour inside cyclone changes. Alumina always gives higher cut size as compare to overall and iron, because of its lighter density.

4.2.5 Effect of Various designs (Du and cone angle Vs D₅₀):

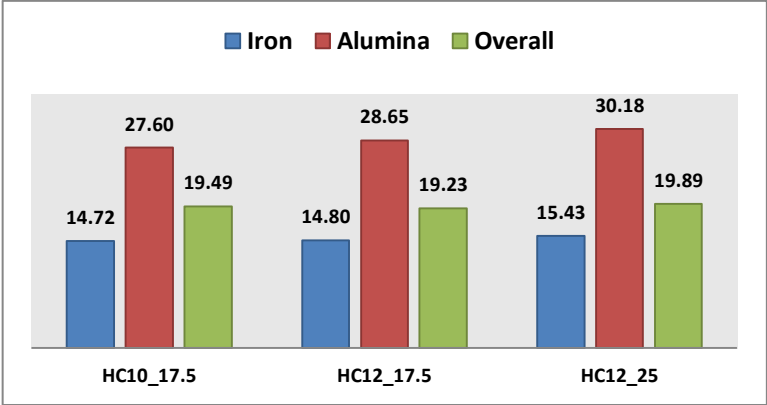


Figure 4.21: Du and cone angle Vs D₅₀

From figure 4.21, comparison of d₅₀ at different designs, the design HC10_17.5 has come up with a better performance as compared to the others. With a lower angle of cone most of the lighter particle i.e. alumina flows through crossflow with higher drag force and efficient separation is obtained.

To understand the interaction of the particle / components in details the further studies were taken in CFD simulations. The detail results are discussions in chapter 5.

Chapter 5

CFD Simulation – Results and Discussions

As described in previous chapter, the multiphase simulations were carried out to understand the volume fraction distribution, mean velocity field, overall classification of the components in hydrocyclone. The multiphase simulation helps in tracking the behavior of flow, its turbulence and the component interactions also. In this section, the multicomponent distribution is focused and the separation efficiency for pure and mixture based component form is studied.

5.1 Two phase flow field:

Using VOF model and RSM turbulence model , the 3 inch hydrocyclone having $D_o =$ mm, $D_u = 12.5$ mm the flow field is solved. Each of the size of silica and magnetite have been provided with different volume fraction with a 10% solid fraction. As shoen in Table 5.1.

Table 5.1: List of cases for feed input attempted for CFD simulation in 3 inch hydrocyclone.

CASES	Proportions (silica : magnetite)	size (micron)	Volume fraction (magnetite)	Volume fraction (Silica)
I	50:50	2.75	0.000455354	0.003642828
		11	0.000455354	0.004926061
		22	0.000668687	0.005349495
		52.32	0.002300606	0.018404848
II	90:10	2.75	0.00222288	0.004445759
		11	0.003005917	0.006011834
		22	0.0032643	0.0065286
		52.32	0.011230769	0.022461538
III	80:20	2.75	0.002517157	0.001029746
		11	0.003403858	0.001392487
		22	0.003696447	0.001512183
		52.32	0.012717563	0.00520264

IV	Pure silica	2.75	0.002517157	0.001029746
		11	0.003403858	0.001392487
		22	0.003696447	0.001512183
		52.32	0.012717563	0.00520264
V	Pure Magnetite	2.75	0.0217	0.000445585
		11	0.1266	0.002599589
		22	0.1364	0.002800821
		52.32	0.5555	0.011406571

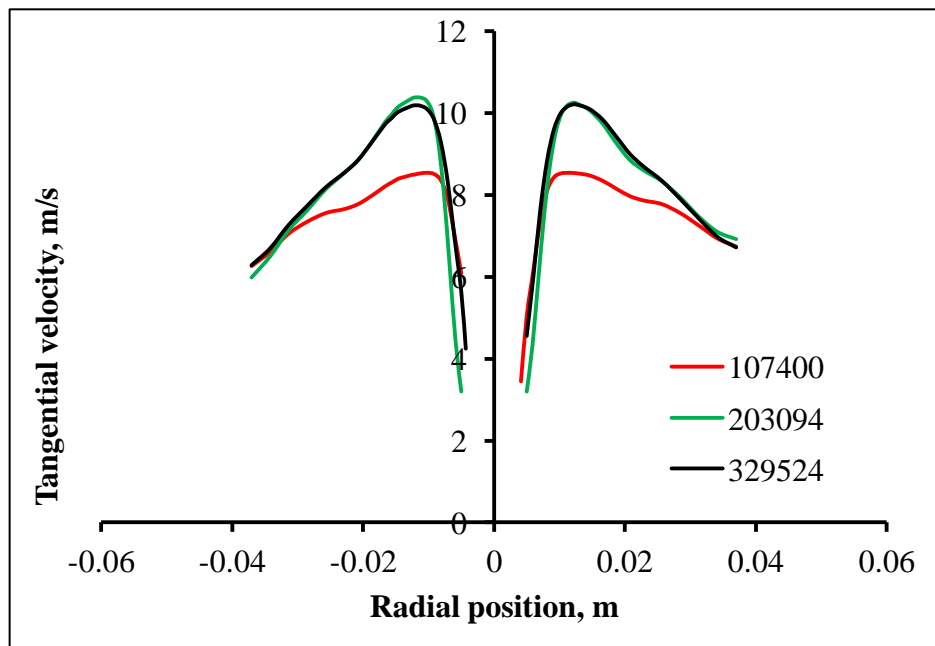


Figure 5.1: Tangential velocities by different meshes at 470 mm from top of the cyclone using RSM and VOF model in 3 inch

The basic CFD approach used as described in chapter 3. The simulations were considered in 3D body fitted grids. To get the optimum grid numbers the grid independence check has been done for the 3inch hydrocyclone at 100 k, 200 k and 400 k (Figure 5.1 and 5.2)

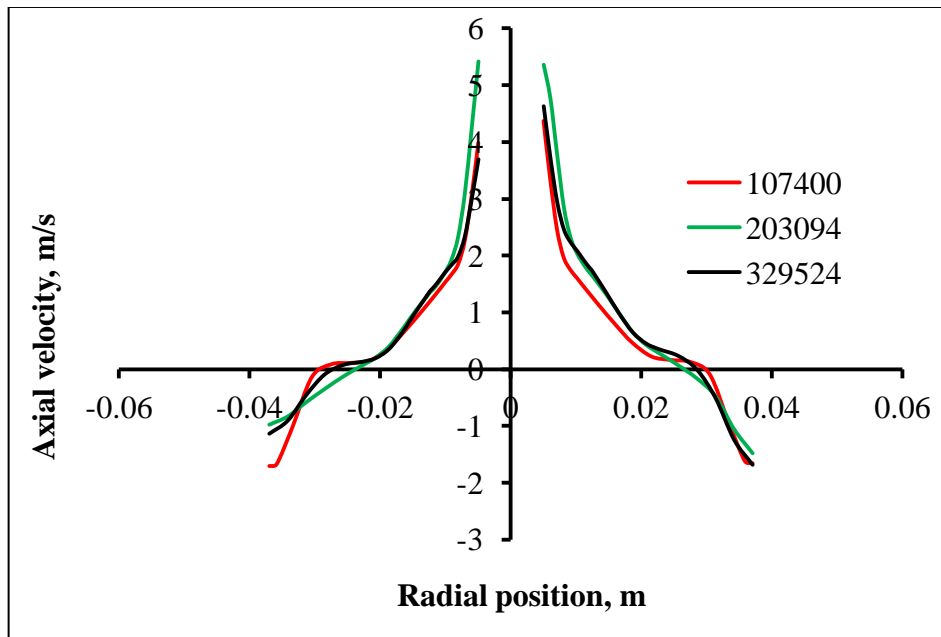


Figure 5.2: Axial velocities by different meshes at 470 mm from top of the cyclone using RSM and VOF model in 3 inch

As we can see from Figure 5.1 and 5.2 200 k gives grid independent, flow field with the optimized number of nodes. Hence for the further studies we will be taking 200 k as optimized grid. The air core for the 2 inch and 3 inch hydrocyclone were obtained from CFD simulation (Figure 5.3). At the same time the turbulence intensity were also compared (Figure 5.4), as 2 inch hydrocyclone have smaller inlet and steep conical section the turbulence intensity recorded was much higher than 3 inch hydrocyclone.

For the initial simulations only water experiments were conducted in 2 inch hydrocyclone and the water flow rate data's were compared it with the experimental data (Figure 5.5). It is found that the simulation and experimental data's are following similar pattern, i.e. with the increase in the pressure at inlet, the flow rate is proportionally increasing.

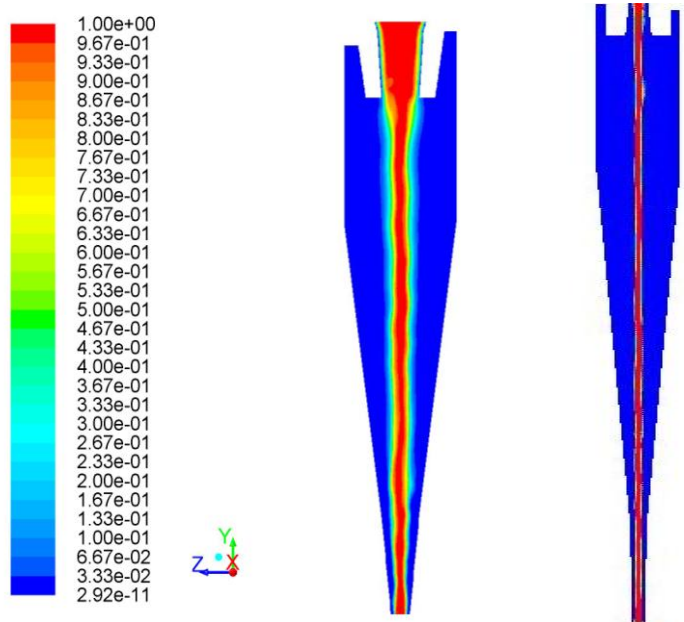


Figure 5.3: Air –core formation in 3inch and 2 inch Hydrocyclone

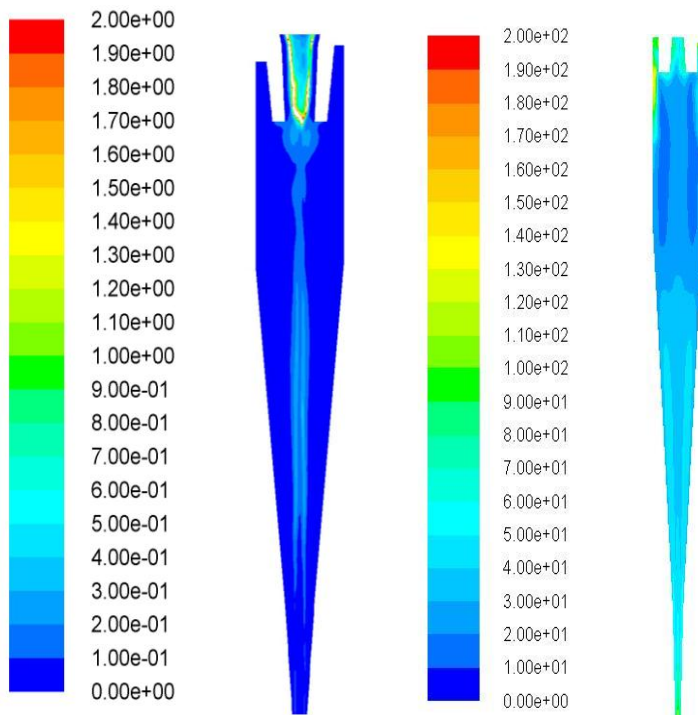


Figure 5.4: Turbulence Intensity in 3inch and 2 inch Hydrocyclone

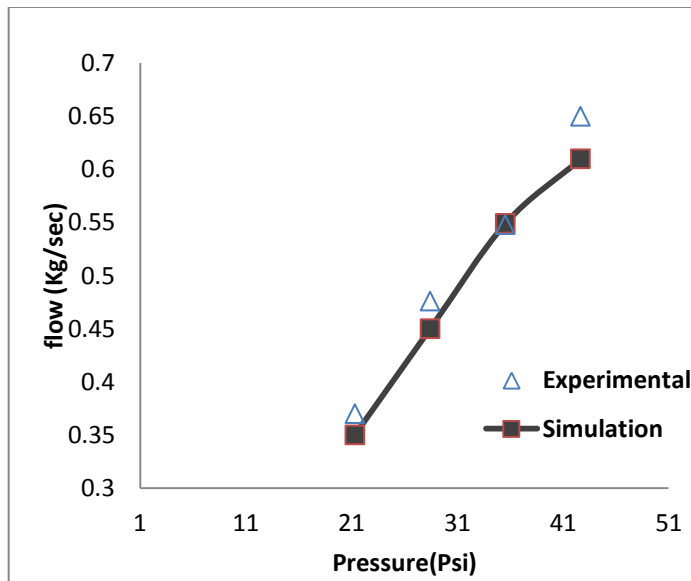


Figure 5.5: Comparison of experimental and CFD plots flow rate Vs Pressure in 2 inch hydrocyclone(6.4 mm Du)

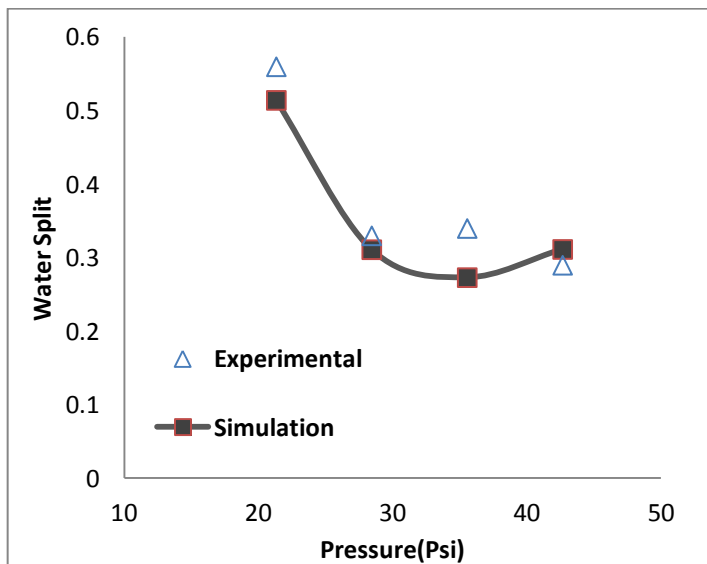


Figure 5.6: Comparison of experimental and CFD plots Water split Vs Pressure in 2 inch hydrocyclone (6.4 mm Du)

Later, 2 inch as well as 3 inch hydrocyclones water only simulations were carried out, for the comparison of CFD and experimental data water split was recorded and found quite good approximation is achieved as shown in figure 5.6 and 5.7. In figure 5.8 the comparison for the air core interphase distribution in simulation are compared with 2 inch and 3 inch hydrocyclones.

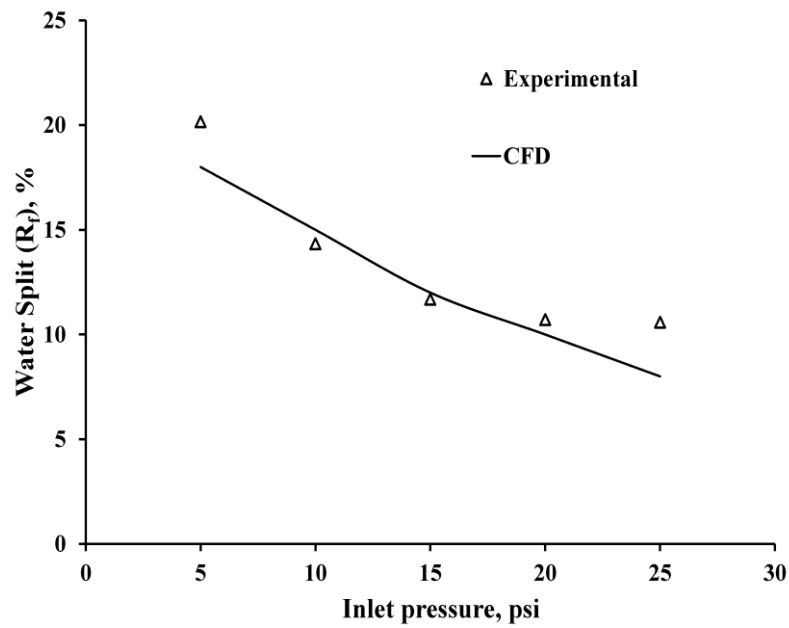


Figure 5.7: water split comparison at different pressures in 3inch hydrocyclone (only water Experiment).

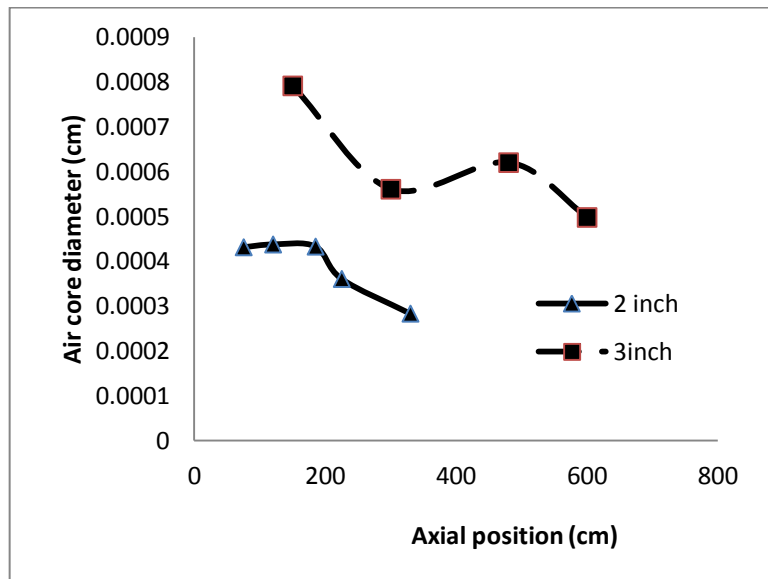


Figure 5.8: Comparison of 2inch and 3 inch hydrocyclone Air core - water interface

5.2 Three inch Hydrocyclone simulations

A. Comparison of volume fraction distribution of silica and magnetite of same size.

With the bi-component mixture as a feed to hydrocyclone the heavier is expected to reach a higher tangential velocity earlier than the lighter one. In the contours below describes and compare the volume fraction of silica (lighter particle) and magnetite (heavier particle) of same sizes at an instant.

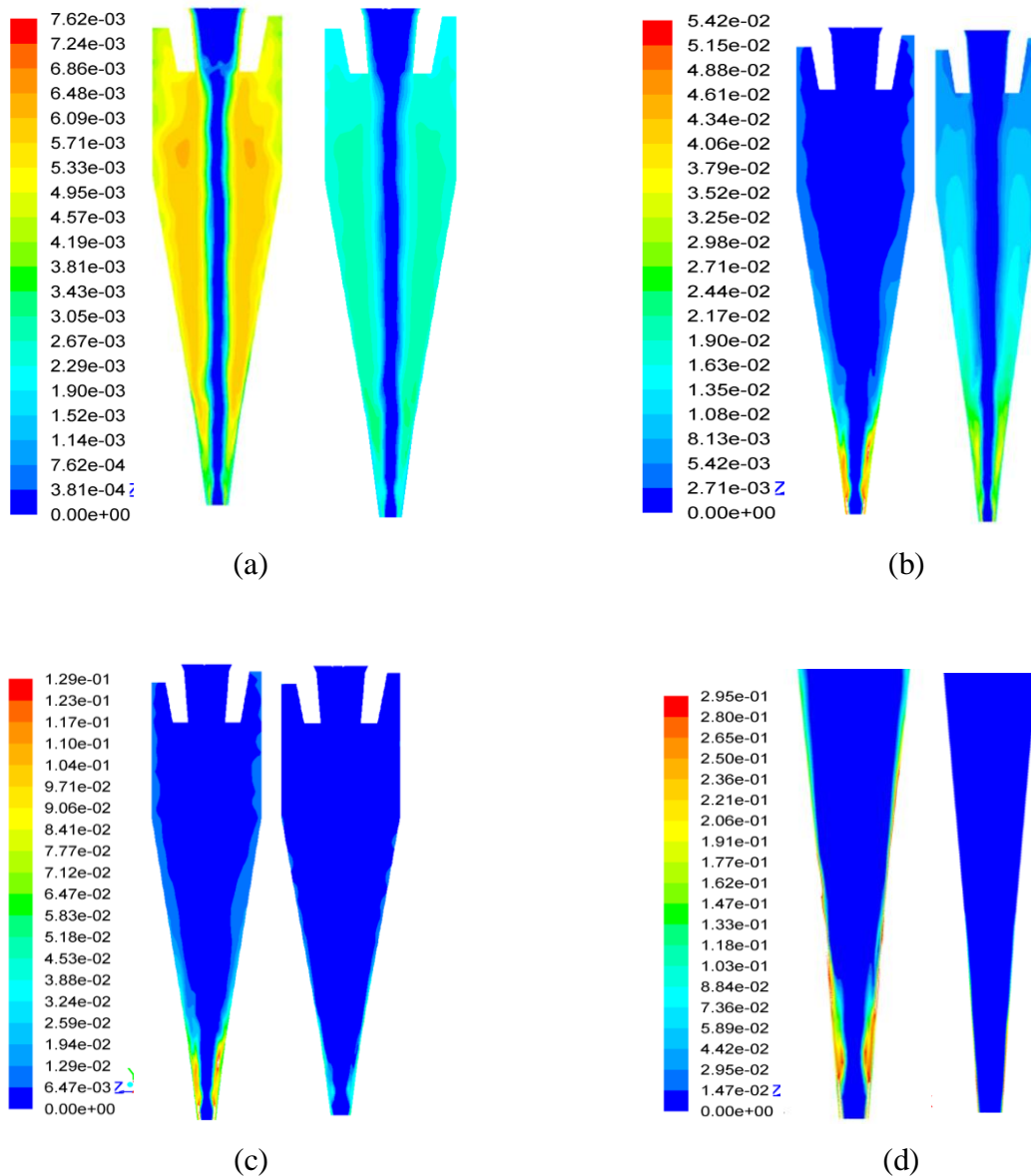


Figure 5.9: Volume fraction contours of silica(left) and magnetite (right) at (a) 2.75 micron, (b) 11 micron, (c) 22 micron and (d) 52.32 micron (From a mixture of 1:1- silica and magnetite)

In this contours it is observed that the time when magnetite is moving faster and occupying the wall side with higher tangential velocity, the silica is still found to be in dispersed inside the flow region. Figure 5.9 (a) Silica and magnetite being at very small size the dispersion is observed for both cases. Figure 5.9(b) illustrates the heavier, magnetite occupying the major fraction in wall side; whereas the silica of same size is dispersed in the fluid regime. With the increase in size (Figure 5.9(c) and 5.9 (d))of the component it is observed that magnetite reports to the underflow higher as compared to the silica.

B. LZVV- locus of zero vertical velocity

Locus of zero vertical velocity (LZVV) is an imaginary line inside the turbulent flow of hydrocyclone where the vertical velocity appears to be zero. According to the equilibrium orbit theory, (Kelsell, (1952)) the particle reporting outside LZVV goes to underflow and the inside one reports to the overflow stream. In Figure 5.10, 4 plot i.e. 50% silica composition, 90% silica composition; pure silica and pure magnetite LZVV are plotted. It is observed that only magnetite LZVV lays out most towards the wall and with the decrease in magnetite % the LZVV shifts towards air-core. This plot also gives a good predict for the silica having higher d_{50} compared to magnetite.

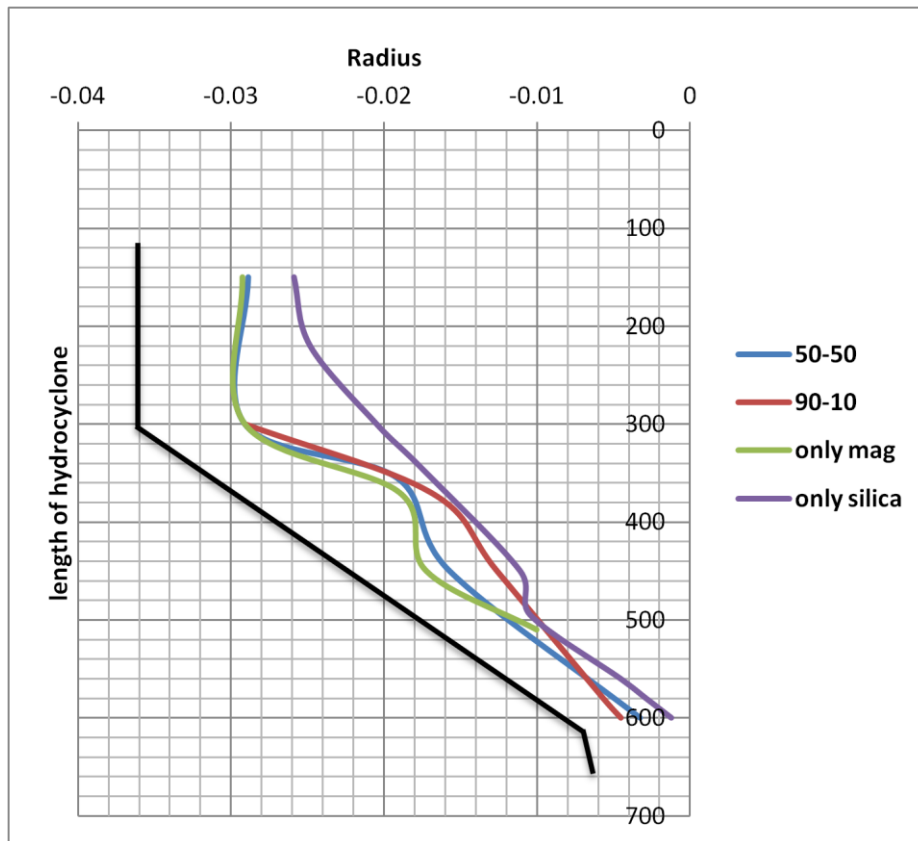


Figure 5.10: LZVV of various proportions of magnetite

C. Tangential velocity plots:

Figure 5.11 and figure 5.12, illustrate the higher density mixture have higher tangential velocities in the flow. Here the pure magnetite showing the highest tangential velocity, among all due the high centrifugal action acting on it. At a height

of 300 mm which is near the intersection of conical and cylindrical portion the velocities in pure magnetite and in the mixtures are found mixing , it is because at that area the separation of the particle and the forces acting are quite mixed, but when it leads to the lower , conical portion (figure 5.12) the magnetite since tends to move down fast, and silica flows towards flow reversal reporting to overflow the tangential velocities is significantly different at various proportions.

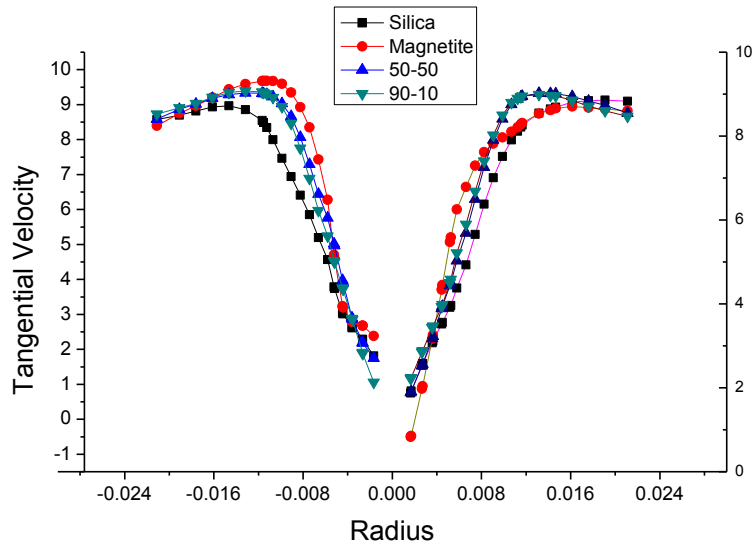


Figure 5.11: Tangential velocity at different proportion at 300 mm from top of hydrocyclone (near the cylindrical and conical junction)

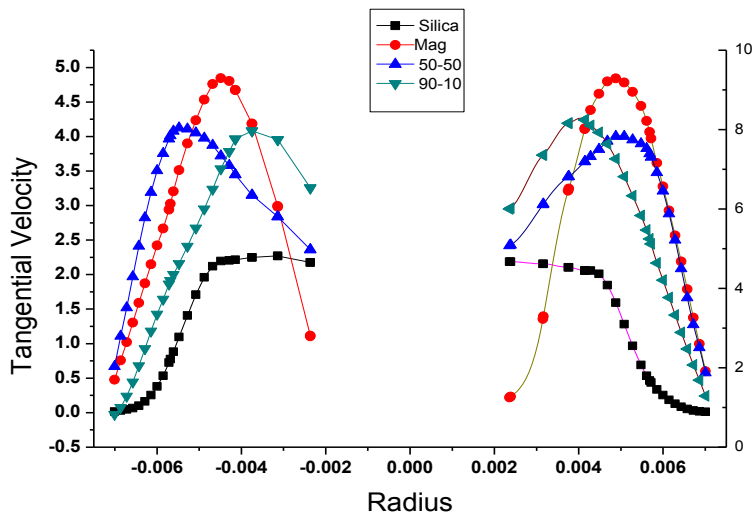


Figure 5.12: Tangential velocity at different proportion at 600 mm from top of hydrocyclone (near spigot)

D. Comparison of vectors –silica at 52.32 micron size at underflow.

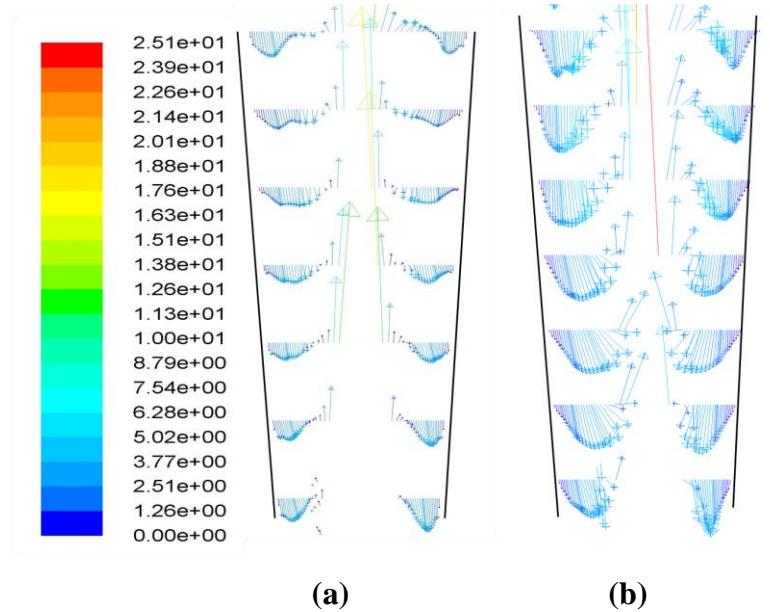


Figure 5.13: Contours for comparison of 52.32 micron size silica in underflow area (a) silica from 1:1 mixture and (b) Pure silica.

In the above (Figure 5.13) of vectors comparison (a) silica of 52.32 micron and (b) silica of pure silica case 52.32 micron reporting to underflow. It is observed that when magnetite is present in mixture it tries to occupy the wall side and pushing the silica particles inwards to the flow, as a result of which the d_{50} of silica increases in mixtures as compared to the pure silica case.

E. Contours at vortex finder

As we discussed in previous arguments the interference of magnetite in a mixture with the silica, it also has been observed at the vortex finder. The Figure 5.14 show the comparison between 9.25 micron particle of (a) silica in 50-50 mixture (b) magnetite in 50-50 mixture (c) pure silica and (d) pure magnetite. Where the finer silica gets short circuited easily in a mixture feed rather than in pure form. While magnetite hence have higher tangential velocity have occupied similar contour in pure and mixed forms at sizes near by the d_{50} .

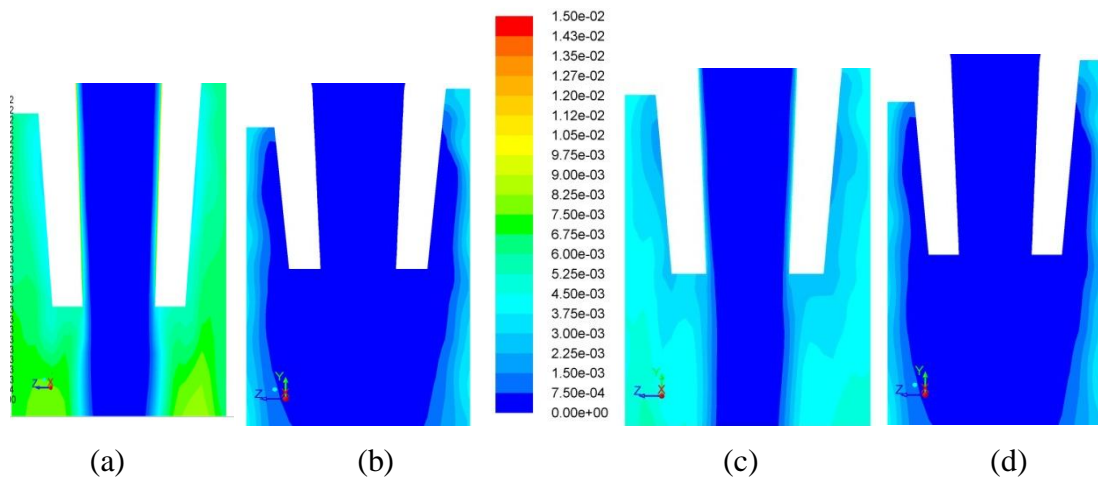


Figure 5.14: Comparison of magnetite and silica distribution at vortex finder area (a), (b) in 50% and (c) pure silica (d) pure magnetite

F. Mean position of Maximum Volume fraction :

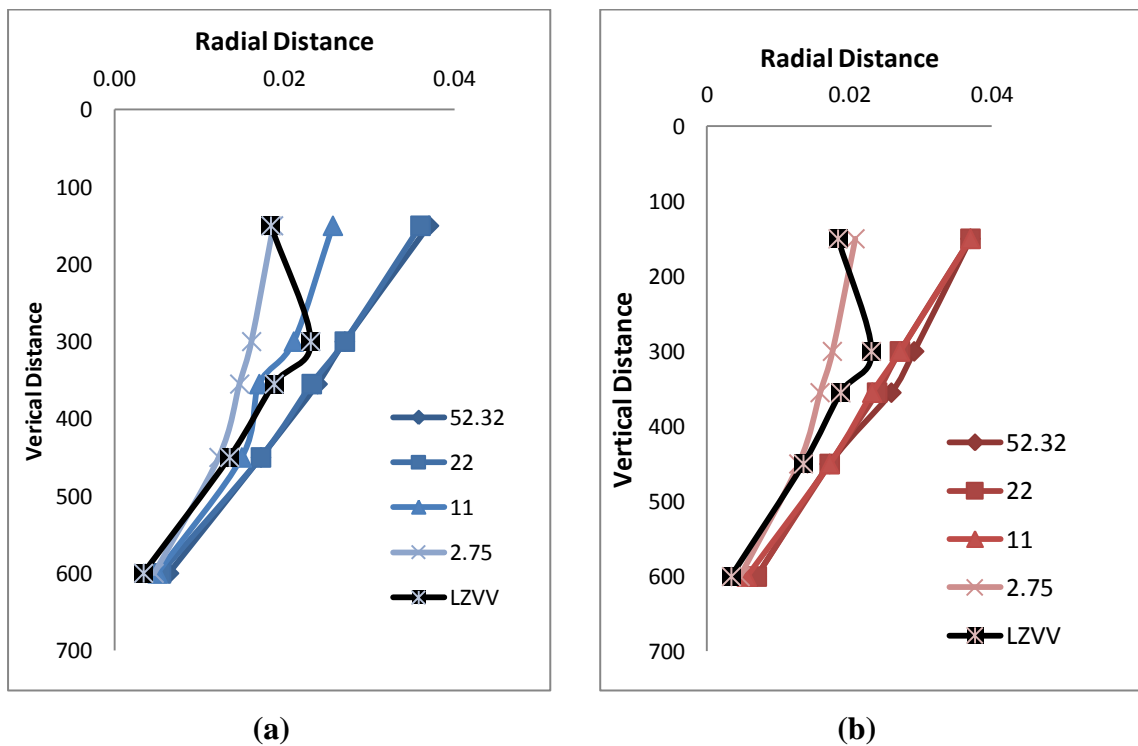


Figure 5.15: Mean position of volume spread (a) silica and (b) magnetite in 1:1 proportion
 In Figure 5.5 the maximum volume fraction's mean position is tracked. This is then compared to the LZVV. The mean position of the maximum volume fraction gives the idea of how and at what position the particles are moving, either to underflow or

overflow. It is observed that the silica of 11 micron reports to overflow but magnetite, 11 micron is reporting to underflow showing the different performances of components in same flow fields. Further studies have considered using pure and with the increase in the magnetite proportion the interaction as shown below.

Comparing Figure 5.16 and Figure 5.17, we can see the difference in the interaction of two components at different proportional inputs. In case of 1:1 proportion (figure 5.16) silica 11 is nearly escaping from the reversal flow, where as in the 8:2 proportion having silica as major portion 11 micron particle directing to the overflow. Whereas, the pure silica's (figure 5.17) cut size has increased sitting between 11 to 22 microns (nearly 11microns), which is also seen in experimental cases. Similarly the magnetite behavior also changes with respect to pure and varying proportions in seen in (b) part of Figure 5.15, 5.16 and 5.17. This is the reason of the magnetite and silica positions at the wall side as discussed in previously.

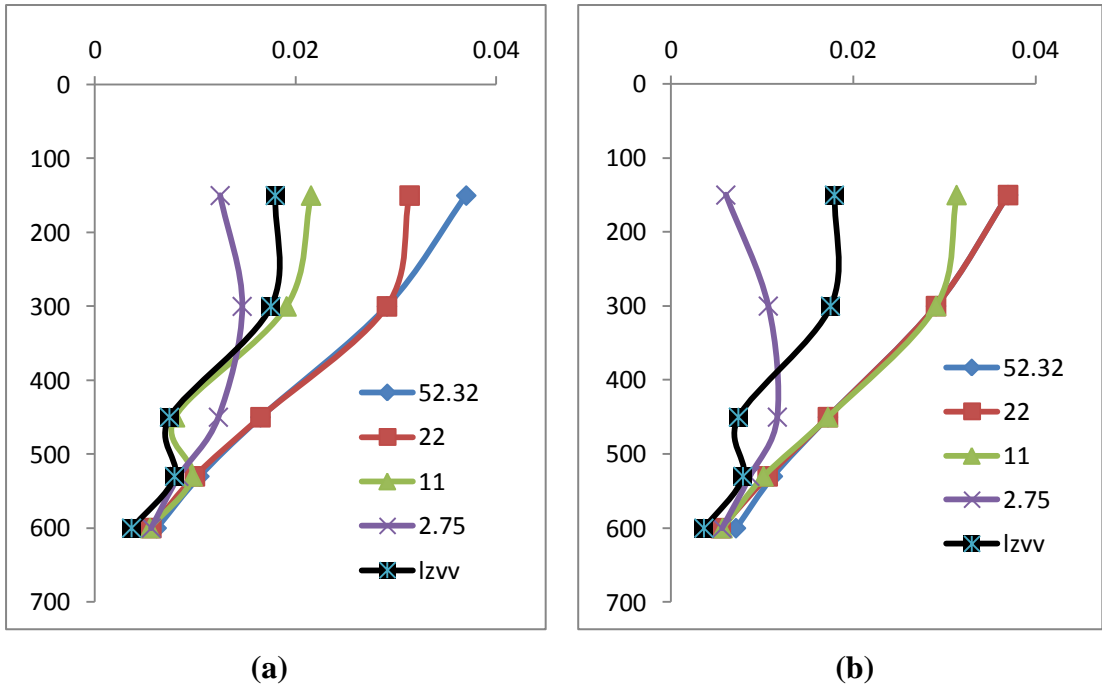


Figure 5.16 :mean position of volume spread (a)silica and (b)magnetite in 8:2 proportion

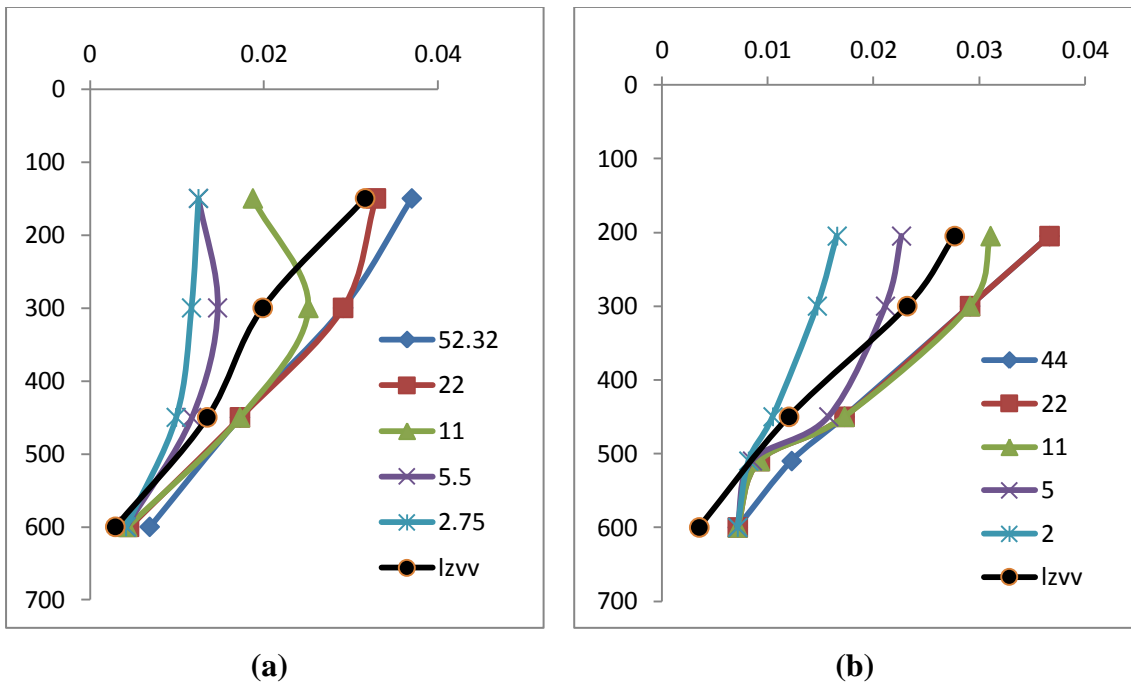


Figure 5.17: Mean position of volume fraction spread (a) pure silica and (b) pure magnetite

Chapter 6

Multicomponent Classification Model testing

As previous studies on multicomponent model in (Narasimha et al, 2014) and (Narasimha et al, 2012) for the performance of hydrocyclone has been described by a set of semi-empirical equations. In IMPC 2014 (Narasimha et al, 2014) the component wise cut-size, sharpness of separation and solid recovery were proposed based on the limited data.

According to the model, the density dependence is considered on accounting the multicomponent behavior. The modified equations by (Narasimha et al, 2014) are as given by Eqn 6.1, 6.2 and 6.3:

6.1 Cut size model:

$$\frac{d_{50}}{D_c} = K_{dl} \left(\frac{D_o}{D_c}\right)^{1.093} \left(\frac{D_u}{D_c}\right)^{-1.0} \left(\frac{(1-f_v)^2}{10^{1.92} f_v}\right)^{-0.703} Re^{-0.936} \left(\frac{D_i}{D_c}\right)^{-0.936} \left(\frac{L_c}{D_c}\right)^{0.187} \left(\frac{1}{\tan(\theta)}\right)^{-0.1988} \left(\frac{(\rho_s - \rho_f)}{\rho_f}\right)^{-1.37} \left(\cos\left(\frac{i}{2}\right)\right)^{-1.034} \quad (6.1)$$

6.2 Sharpness of separation:

$$\alpha = K_{ag} \frac{\left(\frac{D_o}{D_c}\right)^{0.27} \left(\frac{V_t^2}{R_{max} g}\right)^{0.016} \left(\cos\left(\frac{i}{180}\right)\right)^{0.868} \left(\frac{(1-f_v)^2}{10^{1.82} f_v}\right)^{-0.72}}{\left(\frac{D_u}{D_c}\right)^{0.567} \left(\frac{(\rho_s - \rho_f)}{\rho_f}\right)^{1.887} \left(\frac{\mu_m}{\mu_w}\right)^{0.127} \left(\frac{1}{\tan(\theta/2)}\right)^{0.182} \left(\frac{L_c}{D_c}\right)^{0.187}} \pi r^2 \quad (6.2)$$

Also the solid recovery to the underflow is described with respect to the water split to the underflow, R_f . This relation is also associated with function of density of component and the design and operating parameters.

6.3 Solid Recovery model:

$$R_{si} = R_f + A \left(1 - \frac{1}{\rho_{si}}\right)^{0.575} \quad (6.3)$$

Where R_f is taken directly from the literature considering the equation for single component correlation as mentioned in chapter 2.

The validations of these sub generated equations were taken by considering the 32 bi-component experimental data as mentioned in chapter 4.

- A. **Cut size model fitting:** In Figure 6.1, the comparison of current work d_{50} and data of (Plitt, 1980), (Weller et al., 1988), and (Aubrey, 2006) is made. As the figure shows the d_{50} data are well predicted by the model proposed and almost 95% of data lies in the predicted place. Few of the deviation are could be caused because of the size distribution variance during the experimentation.

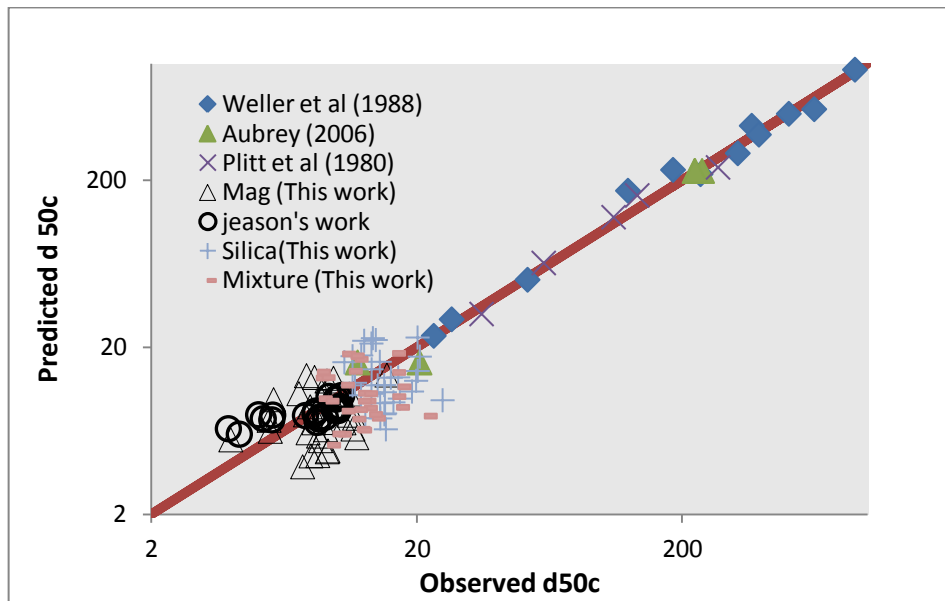


Figure 6.1: d_{50} for the model fitting

B. Solid Component Recovery:

In figure 6.2, the solids component wise recovery data has been fitted. As the magnetite having more centrifugal force towards the wall as observed in previous chapters, the recovery is higher than the silica component. When fitted with the model, it has shown almost 80-90 % data fall in predicted range.

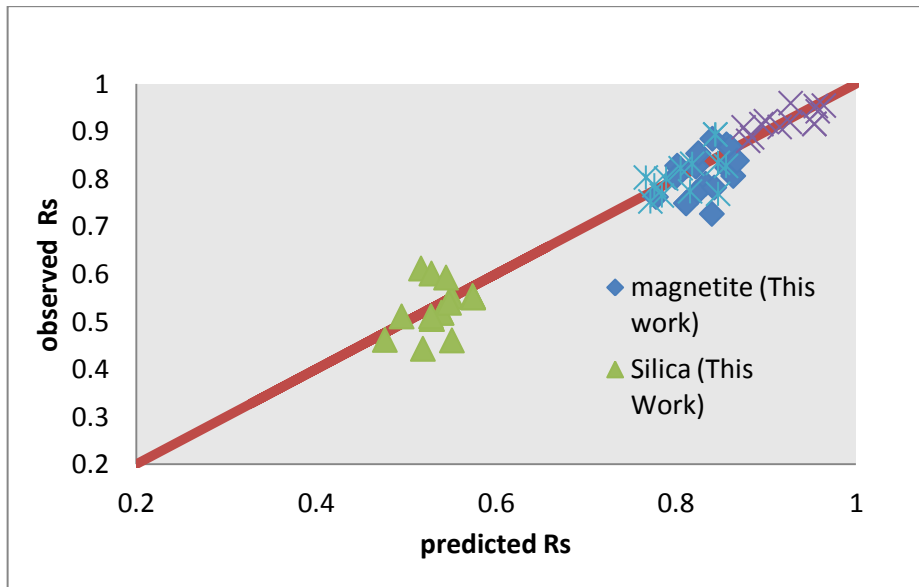


Figure 6.2: Solid recovery for 5% and 10 % experiments

C. Sharpness of separation:

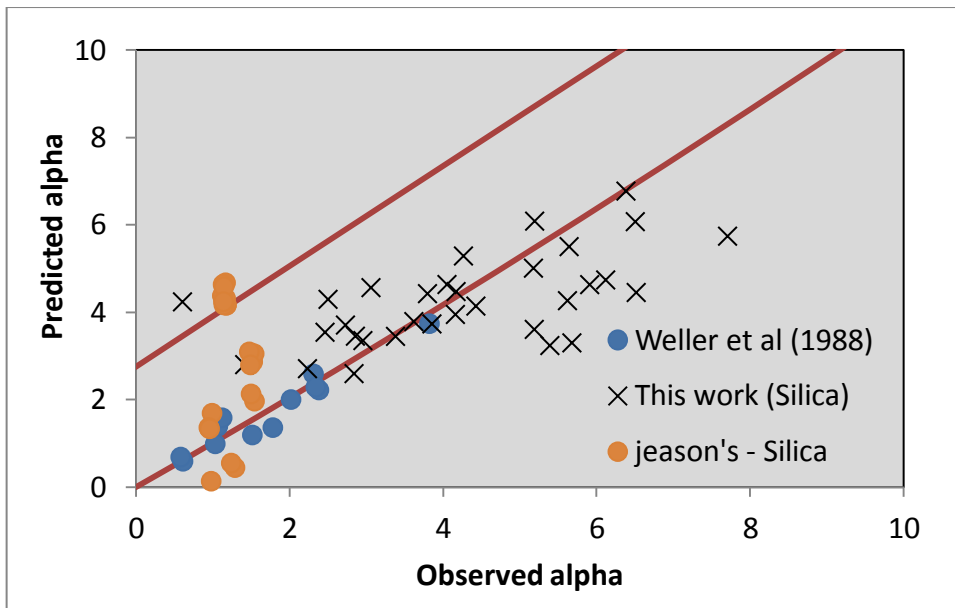


Figure 6.3: Sharpness of separation of silica comparisons with (Weller et al., 1988) and (Narasimha et al., 2014)

As far as the alpha or sharpness of separation concern, with respect to the model prediction to the measured data, high deviation is observed. It has also been observed in previous studies (Jeason's –silica) as shown in figure 6.3. This is expected that it could be because of the high turbulent flow effects in small cone hydrocyclones. Further modification or validation can be approached using the big size cyclone.

Chapter 7

Conclusion and Future work

7.1 Conclusion

In this thesis, multicomponent studies have pursued by experimental and CFD simulation. The performances and parameters were calculated in each case and the interaction and influence of the components on the classifications have studied. This also includes the multicomponent model fitting to (Narasimha et al, 2014).

7.1.1 Bi component studies:

Pure component of magnetite and silica were used, which are easily separable to get the after classification particle distributions in each streams.

The mixtures having 1:9, 2:8, 1:1, 8:2, 9:1 (silica: magnetite) proportions compared with the pure component classification efficiencies. It is observed that the mixtures based components have higher cut-size with respect to pure components.

With the increasing magnetite fraction % the cut-size has comparatively decreased and the silica have shown a vice versa behavior.

Solids recovery (Rs) is observed maximum for magnetite component. At constant feed mixture proportion higher spigots the recovery increases.

With the increase in total solid % and magnetite % in each mixture water split have reduced. The heavier particles reports most to underflow diverting some of the silica particles to the overflow.

7.1.2 Iron Ore Slime Studies:

SEM and XRD analysis is done for the sample characterization at initial stage, describing the morphology and the compound distribution in each stream size-wise chemical analysis is pursued.

The multi-density material i.e. iron and alumina present in iron have shown significant variation in cut- size with respect to the overall feed. Iron shows the lower cut size because high centrifugal force acting on the heaviest particle.

With the change in spigot, the recovery of solid to underflow increases for the larger spigot and a significant increase in the d_{50} has been seen with increase in spigot size.

The new design HC10, which was developed under DST project proved to be potential for reduction of low-density alumina fraction of iron ore slimes

7.1.3 CFD Simulations:

The multiphase CFD approach is done using ANSYS FLUENT, a commercial package. The 10 phases interaction studies have shown the varied volume fraction distribution with respect to pure and mixtures.

The tangential velocities are observed higher in case of magnetite because of higher density attaining higher centrifugal force.

In the mixtures it is observed that the wall side mostly volume is occupied by the magnetite, where heavier components pushes the silica of same size to inwards and hence changing the cut-size of lighter particles. Using CFD simulations of pure and different proportion, LZVV have given an idea that with higher % of magnetite it shifts more towards wall, increasing the cut-size.

The mean position of maximum volume fraction spread studies shows the changing cut-size of silica and magnetite.

7.1.4 Multicomponent Model Validation:

The (Narasimha et al, 2014) model validation have attempted, where component wise d_{50} and R_s have shown quite reasonable predictions. The sharpness of separation have not shown an appreciable fitting, which is expected because of the high turbulent flow regime in the smaller cone.

7.2 Future work

- Experiments on naturally occurring ore for better understanding and fitting of models generated.
- CFD studies for obtaining data for wide range of design and operating conditions.
- Multi-component model tuning and improved to fit sharpness of separation.

References

- Hirt C W, Nichols B D**, Volume of fluid (VOF) method for the dynamics of free boundaries, *J. Comput. Phys.* 39 (1981) 201–225.
- Davailles A, Climent E, Bourgeois F**, Fundamental understanding of swirling flow pattern in hydrocyclones, *Separation Purification Technol.* 92 (2012) 152–160.
- Rakesh A, Kumar Reddy V.T.S.R., Narasimha M.**, Air-core size measurement of operating hydrocyclone by electrical resistance tomography, *Chem. Eng. Technol.* 37 (2014) 795–805.
- Mainza, A, Powell, M S, Knopjes B**, Differential classification of dense material in a three-product cyclone, *Minerals Engineering*, Vol. 17 (2004) 573–579 :
- Hinze J O**, *Turbulence*, New York , USA, (2nd edn) McGraw-Hill(1975).
- Firth B**, coal preparation, Kenmore, Qld, Australia, Energy Technology Division, CSIRO(1984).
- Weller, K.R., Sterns, U.J., Artone, E., Bruckard, W.J**, Multi component models of grinding and classification for scale-up from continuous small or pilot scale circuits, *International journal of Mineral processing*, : Vol. 22 (1988) - 119-147
- Brennan M.S., Narasimha M, Holtham P N**, Multiphase modeling of hydrocyclones – prediction of cut-size, *Mineral Engg*, Vol 20 (2007) 395–406.
- Narasimha M and Jeason Crasta**, Performance of hydrocyclone separating bi-component mixture IMPC, Chile, 2014.
- Narasimha, M, Brennan, Mathew, Holtham P N**, Large eddy simulation of hydrocyclone—prediction of air-core diameter diameter and shape, *International journal of mineral processing*, Vol. 80 (2006) - 1-14.
- Narasimha M**, Multi-component modelling concept for hydrocyclone classifier ,IMPC. - 2012.
- Bhaskar, Udaya K, Murthy, Rama Y, Raju, Ravi M, Tiwari, Sumit, Srivastava J K, Ramakrishnan N**, Characterization and processing of iron ore fines of Kiriburu deposit of India, *International journal of mineral engineering*, Vol. 93 (2000) - 107
- Mahiuddin S**, A study on the beneficiation of Indian iron-ore fines and slime using chemical additives, *International Journal of Mineral Processing*, : Vol. 26 (1989) 3–4 .
- Bradley D., *The Hydrocyclone*. Pergamon Press Ltd, London(1965)

- Manninen M, Taivassalo V, Kallio S**, On the Mixture Model for Multiphase Flow, VTT Publications, Finland, (1996)
- Mohanty S**, Optimization Studies of Hydrocyclone for Beneficiation of Iron Ore Slimes, Mineral Processing and Extractive Metallurgy Review: An International Journal, Vol. 31. (2010) - 2
- Nageswararao, K**, Further developments in the modelling and scale-up of industrial hydrocyclones, Ph.D. Thesis, University of Queensland (JKMRC), Brisbane, Australia(1978).
- Narasimha M**, Improved computational and empirical models for hydrocyclones , JKMRC, The University of Queensland, (2009).
- Narasimha, M, Brennan, M S**, A comprehensive CFD model of dense medium cyclone performance, Mineral Engineering, : Vol. 20 ,(2007) - 414-426 .
- Plitt R**, Mathematical Model of the Hydrocyclone Classifier, CIM Bulletin, Vol 69(776). (1976) - 114-123.
- Kawatra S K**, Significance of Inflections in Hydrocyclone Efficiency Curves in “Advances in comminution”,Society for Mining, Metallurgy, and Exploration, Inc, (2006).
- Smagorinsky J**, General circulation experiments with the primitive equations,American meteorological society, Washington, D.C, General Circulation Research Laboratory,91 (1963) 99–164.
- Wilcox D C**, Turbulence Modelling for CFD,La Canada, CA, USA : DCW Industries Inc., (1994).
- Lynch A J, Rao T C**, Modelling and scale up of hydrocyclone classifiers, In XI IMPC, Cagliari,(1975) pp. 9-25
- Napier-Munn T J, Morrell S, Morrison R D, Kojovic T**, Mineral Comminution Circuits—Their Operation and Optimisation, In JKMRC Monograph Series, Julius Kruttschnitt Mineral Research Centre, University of Queensland.(1996)
- Smagorinsky J**, General circulation experiments with the primitive equations,American meteorological society, Washington, D.C, General Circulation Research Laboratory,91 (1963) 99–164.

Boysan F, Ayers W H, Swithenbank J, A fundamental mathematical modelling approach to cyclone design, Institution of Chemical Engineers, 21(1982), Pg 222-230

Dyakowski and Williams, Modelling turbulent flow within a small-diameter hydrocyclone , vol 48(1993) Pg -1143-1152

Malhotra A, Branion R M R, Hauptmann E G, Modelling the flow in a hydrocyclone, vol -72 (1994), Pg:953-960

Nowakowska A F, Cullivan J C, Williams R A, Dyakowski T, Application of CFD to modelling of the flow in hydrocyclones. Is this a realizable option or still a research challenge?, Vol-17, (2004), Pg-661-669

Slack M D, Prasad R O, Bakker A, Boysan, Advances in cyclone modelling using unstructured grids, Chem Eng, 78 (2000), pp. 1098–1104

Cullivan J C, Williams R A, Cross C R, Understanding the hydrocyclone separator through computational fluid dynamics, Chemical Engineering, Research and Design, Vol-81 (2003), pp. 455–466

Ma L, Ingham D B, Wen X, Numerical modelling of the fluid and particle penetration through small sampling cyclones, Journal of Aerosol Science, Vol-31 (2000), pp. 1097–1119.